Time Integration of Diapycnal Diffusion and Richardson Number Dependent Mixing in Isopycnal Coordinate Ocean Models

Robert Hallberg

NOAA Geophysical Fluid Dynamics Laboratory
Princeton University, Forrestal Campus, U.S. Route 1, P.O. Box 308,
Princeton, New Jersey 08542

February 26, 1999

Address for correspondence: Dr. Robert Hallberg, NOAA GFDL, Princeton University, Forrestal
Campus, US Route 1, P.O. Box 308, Princeton, NJ 08542
e-mail: rwh@gfdl.gov

Abstract

In isopycnal coordinate ocean models, diapycnal diffusion must be expressed as a nonlinear difference equation. This nonlinear equation is not amenable to traditional implicit methods of solution, but explicit methods typically have a time step limit of order $\Delta t \leq h^2 / \kappa$ (where Δt is the time step, h is the isopycnal layer thickness, and κ is the diapycnal diffusivity), which cannot generally be satisfied since the layers could be arbitrarily thin. It is especially important that the diffusion time integration scheme have no such limit if the diapycnal diffusivity is determined by the local Richardson number. An iterative, implicit time integration scheme of diapycnal diffusion in isopycnal layers is suggested. This scheme is demonstrated to have qualitatively correct behavior in the limit of arbitrarily thin initial layer thickness, is highly accurate in the limit of well resolved layers, and is not significantly more expensive than existing schemes. This approach is also shown to be compatible with an implicit Richardson number dependent mixing parameterization, and to give a plausible simulation of an entraining gravity current with parameters like the Mediterranean Water overflow through the Straits of Gibraltar.

1. Introduction

In geopotential coordinate ocean models, time integration of the vertical diffusion equation is fairly simple. Vertical diffusion is described by a linear equation, and an implicit time stepping scheme for vertical diffusion in geopotential coordinates is easily implemented by solving a tridiagonal equation and is stable for any time step and vertical resolution. In many cases the vertical resolution is sufficiently coarse that the time steps set by other processes can even be used safely with an explicit discretization of vertical diffusion. By contrast, when density is the vertical coordinate of an ocean model, the vertical diffusion equation is much more difficult to integrate in time. Implicit integration of the diapycnal diffusion equation in isopycnal coordinates is complicated by the fact that this equation is nonlinear, and since the vertical resolution migrates with the flow there is no guarantee that the vertical resolution is sufficiently coarse to permit an explicit time integration.

Vertical advection in geopotential coordinates is often thought of as independent of diapycnal diffusion, whereas its counterpart in isopycnal coordinates, diapycnal advection (motion of fluid across isopycnal surfaces), is the direct result of diapycnal diffusion. The nonlinearity of diffusion in the isopycnal layer thickness equation is the counterpart of the nonlinear vertical advection of density in geopotential coordinates.

Isentropic coordinate atmospheric models do not suffer quite the same difficulty as isopycnal coordinate ocean models because radiative transfer and moist convection act to restore the (dry) atmospheric stratification much more efficiently than does thermal diffusion in the ocean.

An explicit time integration scheme is inadequate for an isopycnal coordinate model because it is subject to the time step limit $\kappa \Delta t / h^2 < 1/2$ for stability, where κ is the diapycnal diffusivity, Δt is the time step, and h is the layer thickness. Since there should be no lower bound on the thickness of a layer, it is impossible to satisfy this constraint in all cases, even if κ is constant. If κ is determined by the local gradient Richardson number, a very large κ may be indicated precisely where h is smallest. Hu (1996a) avoids this constraint by calculating the diapycnal buoyancy flux using the average density gradient over a specified distance from the center of a layer (typically 20 m) if the layer is thinner than this distance. (The Hu scheme is used in some versions of the Miami Isopycnic Coordinate Ocean Model, and in simulations by Hu (1996b).) This solution suffers from being potentially an O(N^2) operation for each horizontal grid point, where N is the number of layers, and from having quantized buoyancy fluxes when the layers are thin. Oberhuber (1993) calculates the entrainment rate of each layer implicitly, but the entrainment in each layer is independent of the entrainment in adjacent layers. Oberhuber's approach can lead to spuriously vanishing layers if the diffusivity (or in his construction the layer turbulent kinetic energy) differs significantly between adjacent layers, requiring a corrective step in his time discretization. McDou-

gall and Dewar (1998) mention the step limitation of explicit integration in their exploration of the discretization of diapycnal diffusion in isopycnal coordinate models but offer no solution.

It should be noted that the ocean's interior is characterized almost everywhere by diffusive timescales that are extremely long compared with the other characteristic timescales of the flow, such as the inertial period. In such situations any time integration scheme will work well for describing diapycnal diffusion in an isopycnal coordinate model, and it is no more difficult to represent diapycnal mixing than it would be in a depth-coordinate model. The techniques described here reproduce the proper solutions in this most common case where diffusion operates slowly, while also giving sensible results in those situations where diapycnal mixing is vigorous.

The time step limit with explicit time integration of diapycnal diffusion is a particularly acute problem for incorporation of Richardson number dependent mixing (or another form of model-state dependent mixing). With a forwards scheme, entrainment must somehow be limited to keep the neighboring layers from developing negative thickness, and this limit severely restricts the utility of Richardson number dependent mixing for describing instances of intense and strongly spatially varying entrainment. It is not clear that an effective Richardson number entrainment scheme can be implemented in an isopycnal coordinate model without using some form of implicit time integration.

But some form of model-state dependent mixing is critical for some oceanographically important phenomenon. For example, entraining gravity currents are extremely important for determining the watermass properties that are found in the open ocean, and strongly nonlinear entrainment is absolutely essential for reproducing the observed transport and density variations along the plume (Price and Baringer, 1994). The recent DYNAMO project finds that a lack of entrainment in the gravity currents downstream of flow over sills is one of the most acute deficiencies of the isopycnal coordinate model they use (The DYNAMO Group, 1997). Similarly, it is generally accepted that the combination of small-scale turbulence and resolvable shears is responsible for the vigorous mixing in the subsurface equatorial ocean, and that the resolvable Richardson numbers rarely drop below a critical threshold value (Peters et al., 1995).

The isopycnal coordinate models in most common use are coupled to a variable density surface bulk mixed layer (Bleck et al., 1992; Oberhuber 1993). The surface mixed layer is, by definition, unstratified and hence would always represented by just one or two isopycnal layers (if the mixed layer density falls between the prescribed layer densities). Unlike geopotential or sigma coordinate ocean models, a pure isopycnal coordinate ocean model will never be able to resolve the vertical structure of the mixed layer. Sea surface temperature is often a critical field either for coupling an ocean model with a model atmosphere or for calculating the surface buoyancy flux, but with a pure isopycnal coordinate model sea surface temperatures would have abrupt jumps where the layers outcrop. Also, it is difficult to apply separate heat and fresh water flux surface boundary conditions without a bulk mixed layer - they may nearly compensate each other, requiring mechan-

ical mixing to the correct depth to give accurate tendencies of sea surface temperature and salinity. When the surface structure is of interest or a nontrivial equation of state is used, it is advisable to use a bulk surface mixed layer. The turbulent mixing schemes described here for use in the interior and in the bottom boundary layer are probably only useful for the surface mixed layer as well for idealized geophysical fluid dynamics studies.

The present work suggests an implicit time integration technique for diapycnal diffusion in isopycnal coordinate ocean models. When the diffusivity of a layer is specified, two schemes are suggested for the entrainment rate of a layer given the entrainment rates of neighboring layers. These schemes are essentially implementations of the dual-entrainment approach of Oberhuber (1993) and McDougall and Dewar (1998), in which each layer simultaneously entrains both from above and below, and both diapycnal diffusion and advection are simultaneously described. These schemes give qualitatively correct results in all parts of parameter space. If a very long time step is used, a modified iterative technique may be used to give arbitrarily accurate solutions, otherwise a simple implicit technique gives reasonable results. Using an estimate of the derivative of each layer's entrainment rate with respect to the entrainment rates of neighboring layers, a Newton's method based vertical iteration, subject to constraints to impose surface and bottom flux boundary conditions, is used to update the estimate of layer entrainment rates. This approach is shown to give qualitatively accurate entrainment rates in difficult cases, even after just the first iteration, and converges to an exact solution with multiple iterations. With one iteration, this scheme is only moderately more expensive than an explicit time integration scheme for diffusion with limits to keep the layer thicknesses from becoming negative, and avoids numerical instabilities due to diapycnal diffusion. A partially implicit layer Richardson number dependent entrainment scheme can be combined with the diffusive layer entrainment scheme, and such an approach is shown to give reasonable entrainment in a simple model of a gravity current, whereas an equivalent explicit scheme is wholly inadequate.

2. Diapycnal diffusion in isopycnal coordinate models

McDougall and Dewar (1998) present an excellent derivation of an appropriate discretization for diapycnal diffusion in isopycnal coordinate models with both temperature and salinity as state variables. Only a very brief reprise of that work is presented here, and for simplicity density is assumed to be a state variable. The time integration techniques presented here are entirely consistent with the McDougall and Dewar (1998) discretization.

The Boussinesq continuity equation and the density equation,

$$\nabla \cdot \boldsymbol{U}_3 = 0 \text{ and } \frac{D\rho}{Dt} = \nabla \cdot (\kappa \nabla \rho) \tag{2.1}$$

(here U_3 is the three dimensional velocity, ρ is potential density and κ is the Fickian diapycnal diffusivity), can be combined to give the continuity equation in isopycnal coordinates:

$$\frac{\partial}{\partial t}\left(\frac{\partial z}{\partial \rho}\right) + \nabla_\rho \cdot \left(u\frac{\partial z}{\partial \rho}\right) = -\frac{\partial}{\partial \rho}\left(\frac{\partial z}{\partial \rho}\frac{D\rho}{Dt}\right) \tag{2.2}$$

$$\approx -\frac{\partial}{\partial \rho}\left(\frac{\partial z}{\partial \rho}\frac{\partial}{\partial z}\left(\kappa\frac{\partial \rho}{\partial z}\right)\right) = -\frac{\partial}{\partial \rho}\left(\frac{\partial}{\partial \rho}\left(\kappa\frac{\partial \rho}{\partial z}\right)\right)$$

The only approximations here are that only diapycnal diffusion alters the density of a fluid parcel and that the slope of isopycnals is sufficiently small that the total density gradients are well approximated by just the vertical gradients. Both of these assumptions are well justified for the ocean at mesoscales and larger except in regions of active convection. If (2.2) is integrated in density between $\rho_{k-1/2}$ and $\rho_{k+1/2}$ and the layer thickness is defined as

$$h_k \equiv -\int_{\rho_{k-1/2}}^{\rho_{k+1/2}}\frac{\partial z}{\partial \rho}d\rho , \tag{2.3}$$

the layer continuity equation results:

$$\frac{\partial h_k}{\partial t} + \nabla_\rho \cdot (u_k h_k) = \frac{\partial}{\partial \rho}\left(\kappa\frac{\partial \rho}{\partial z}\right)\bigg|_{k+1/2} - \frac{\partial}{\partial \rho}\left(\kappa\frac{\partial \rho}{\partial z}\right)\bigg|_{k-1/2} \tag{2.4}$$

$$\approx \frac{1}{\rho_{k+1} - \rho_k}\left[\left(\kappa\frac{\partial \rho}{\partial z}\right)_{k+1} - \left(\kappa\frac{\partial \rho}{\partial z}\right)_k\right] - \frac{1}{\rho_k - \rho_{k-1}}\left[\left(\kappa\frac{\partial \rho}{\partial z}\right)_k - \left(\kappa\frac{\partial \rho}{\partial z}\right)_{k-1}\right]$$

Finally, the vertical buoyancy flux in interior layers can be discretized consistently as

$$-\left(\kappa\frac{\partial \rho}{\partial z}\right)_k = \frac{\kappa_k(\rho_{k+1/2} - \rho_{k-1/2})}{h_k} \equiv \frac{\kappa_k\Delta\rho_k}{h_k} . \tag{2.5}$$

Here the definition of κ_k would include the difference between the inverse of the average h over a grid cell and the average of $(1/h)$ over that cell. Since the buoyancy fluxes are defined only for each layer, any buoyancy flux boundary conditions must be applied to the top and bottom layers, as will be described in section §4. Combining (2.4) and (2.5) with the definition $\Delta\rho_{k+1/2} \equiv \rho_{k+1} - \rho_k$ gives the final form of the diffusive continuity equation:

$$\frac{\partial h_k}{\partial t} + \nabla_\rho \cdot (u_k h_k) \tag{2.6}$$

$$= \frac{1}{\Delta\rho_{k-1/2}}\left(\frac{\kappa_k\Delta\rho_k}{h_k} - \frac{\kappa_{k-1}\Delta\rho_{k-1}}{h_{k-1}}\right) - \frac{1}{\Delta\rho_{k+1/2}}\left(\frac{\kappa_{k+1}\Delta\rho_{k+1}}{h_{k+1}} - \frac{\kappa_k\Delta\rho_k}{h_k}\right)$$

Introducing the layer buoyancy flux, F_k, defined by

$$F_k \equiv \frac{\kappa_k\Delta\rho_k}{h_k} , \tag{2.7}$$

and the thickness loss from layer k due to the fluxes in the neighboring layers, G_k, defined by

$$G_k \equiv \frac{F_{k-1}}{\Delta\rho_{k-1/2}} + \frac{F_{k+1}}{\Delta\rho_{k+1/2}}, \tag{2.8}$$

(2.6) becomes

$$\frac{\partial h_k}{\partial t} + \nabla_\rho \cdot (\boldsymbol{u}_k h_k) = \frac{F_k - F_{k-1}}{\Delta\rho_{k-1/2}} - \frac{F_{k+1} - F_k}{\Delta\rho_{k+1/2}} \tag{2.9}$$

$$\equiv \left(\frac{1}{\Delta\rho_{k-1/2}} + \frac{1}{\Delta\rho_{k+1/2}}\right) F_k - G_k$$

There can be no mass flux through the upper surface of the topmost layer or the bottom surface of the bottommost layer, so the first and second terms on the right hand side of the first line of (2.9) are omitted in the top and bottom layers respectively.

As shown by Oberhuber (1993) and McDougall and Dewar (1998), a dual-stream upstream discretization for the entrainment of density (or any other state variable that is conserved upon mixing) guarantees that the density of each layer is conserved with a linear equation of state. With the dual-stream entrainment parameterization, both diapycnal diffusion and diapycnal advection are simultaneously described by fluid moving both upwards and downwards across every interior interface in appropriate ratios. Oberhuber (1993) further utilizes the dual-entrainment scheme to compensate for any discrepancies between the modeled layer density and the preordained target layer density by adjusting the ratio of the entrainment by a layer from the layers above and below. The density conservation equation,

$$\frac{\partial}{\partial t}(\rho_k h_k) + \nabla_\rho \cdot (\boldsymbol{u}_k h_k \rho_k) = \frac{F_k \rho_{k-1} - F_{k-1}\rho_k}{\Delta\rho_{k-1/2}} - \frac{F_{k+1}\rho_k - F_k\rho_{k+1}}{\Delta\rho_{k+1/2}} \tag{2.10}$$

can be combined with (2.9) to give

$$h_k \frac{\partial \rho_k}{\partial t} = \rho_k \left[\frac{F_k - F_{k-1}}{\Delta\rho_{k-1/2}} - \frac{F_{k+1} - F_k}{\Delta\rho_{k+1/2}} - \frac{\partial h_k}{\partial t} - \nabla_\rho \cdot (\boldsymbol{u}_k h_k) \right] + F_k \left(\frac{\Delta\rho_{k+1/2}}{\Delta\rho_{k+1/2}} - \frac{\Delta\rho_{k-1/2}}{\Delta\rho_{k-1/2}}\right) \tag{2.11}$$

$$= 0$$

showing that the layer density is constant with the dual-entrainment upstream discretization. This property holds regardless of the scheme used to solve (2.10) in time. For temperature or salinity, an implicit time discretization of the appropriate counterpart to (2.10) (calculating horizontal advection separately) is both necessary and easy to implement.

If there is a nonlinear equation of state, the density or potential density of a layer will not be guaranteed to be perfectly constant after diapycnal mixing. The layer density will also vary due to cabbeling arising from along-isopycnal mixing. These discrepancies may be addressed by an appropriate, conservative vertical remapping (which is essentially what McDougall and Dewar

(1998) advocate), or it may be addressed as a part of the vertical mixing, as Oberhuber (1993) does. Ignoring horizontal advection, an implicit time discretization of (2.10) with the ratios of entrainment from above and below modified (along the lines used by Oberhuber (1993)) to correct for density deviations can be written as

$$
\frac{\rho_k^{n+1}h_k^{n+1} - \rho_k^n h_k^n}{\Delta t} = \frac{(F_k + \tilde{F}_k)\rho_{k-1}^{n+1} - (F_{k-1} - \tilde{F}_{k-1})\rho_k^{n+1}}{\Delta\rho_{k-1/2}}
$$
$$
- \frac{(F_{k+1} + \tilde{F}_{k+1})\rho_k^{n+1} - (F_k - \tilde{F}_k)\rho_{k+1}^{n+1}}{\Delta\rho_{k+1/2}} \tag{2.12}
$$

It can easily be shown that ρ_k^{n+1} will agree with a layer target density $\widehat{\rho_k}$ if

$$
\tilde{F}_k = \frac{h_k^n}{2\Delta t}(\rho_k^n - \widehat{\rho_k}), \tag{2.13}
$$

For the stability of (2.12), the corrective flux must be less than the minimum flux that a layer will have averaged over a time step, so for an interior layer (2.13) must be replaced by

$$
\tilde{F}_k = min\left(\frac{h_k^n}{2\Delta t}(\rho_k^n - \widehat{\rho_k}), \left\{\left[(h_k^n)^2 + 2\kappa\Delta t\left(\frac{\Delta\rho_k}{\Delta\rho_{k+1/2}} + \frac{\Delta\rho_k}{\Delta\rho_{k-1/2}}\right)\right]^{1/2} - h_k^n\right\}\right) \tag{2.14}
$$

or a more restrictive limit. This corrective flux is not perfect, both because its magnitude is limited in thick and weakly diffusive layers, and because of nonlinearities in the equation of state, but it will cause the layer densities to be damped towards the target densities. These corrective fluxes would calculated before any vertical iteration, and their inclusion is straightforward in all of the developments that follow, so they will be omitted henceforth for the sake of clarity. If the density anomalies are not predominantly due to errors in the diapycnal mixing, an minimally diffusive vertical remapping would be the preferred remapping. Even with the corrective fluxes, occasional vertical remapping may still prove necessary to correct layer density discrepancies, depending on the characteristics of a particular flow.

In geopotential coordinates diffusion is described by a linear equation, and it is always possible to choose a diffusivity and time step which are small enough that an explicit discretization of diffusion is stable. Alternately, it is trivial to implement an implicit discretization of diffusion in one dimension with standard techniques. In isopycnal coordinates, diapycnal diffusion is described by a nonlinear equation, and it is possible for a flow to evolve into a state (with very thin layers) in which an explicit discretization of diffusion is unstable, regardless of how small the diffusivity or time step. It is absolutely essential to use an implicit discretization of the right hand side of (2.6), but standard (linear) techniques cannot handle this nonlinear equation.

The fundamental difference between diapycnal diffusion in geopotential coordinates (or other fixed coordinates) and diapycnal diffusion in isopycnal coordinates is that isopycnal coordinates make the physically meaningful connection between diapycnal advection and diapycnal dif-

fusion, through the dual-entrainment scheme, while in fixed coordinates these two processes are separate. The nonlinear diapycnal advection term in fixed coordinates is in some sense responsible for the nonlinearity of diffusion in Lagrangian (isopycnal) coordinates. This physically well-motivated combination of diapycnal advection and diffusion is largely responsible for the exceedingly valuable adiabatic nature of an isopycnal coordinate model, but it demands a sophisticated treatment of diapycnal diffusion to be able to accurately handle all realizable situations. The remainder of the paper presents a suitable time integration technique for diapycnal diffusion in isopycnal coordinates.

3. Integrating the equation for a single layer

If the diffusive buoyancy fluxes (F_k) in neighboring layers are known, and the density differences between the layers are equal, the diffusive continuity equation (neglecting horizontal advection) for layer k, (2.6), becomes

$$\frac{\partial h_k}{\partial t} = \frac{2\kappa_k}{h_k} - \frac{F_{k-1}}{\Delta\rho} - \frac{F_{k+1}}{\Delta\rho} \equiv \frac{2\kappa_k}{h_k} - G_k. \tag{3.1}$$

This is a fairly simple equation, but it is not one that is commonly encountered, so it is worthwhile to briefly discuss several options for integrating this equation numerically. An arbitrarily accurate, iterative solution technique is described first. This scheme is useful both for consideration for use in ocean models and as a standard against which to judge other time integration techniques. A number of algebraic discretizations of (3.1) are described next. These schemes are less computationally demanding and are the most likely to be useful for ocean models. All of these schemes give accurate results when diffusive timescales are long, as is the case in much of the ocean's volume. The distinction between the schemes arises in the uncommon, but oceanographically important, case where mixing timescales are relatively short.

An exact iterative solution for one layer

Eq. (3.1) can be integrated analytically in time for Δt starting at a thickness $h_{k,0}$ to give a closed form implicit solution for $h_{k,t} \equiv h_k(\Delta t)$ provided that $G_k > 0$:

$$h_{k,t} - h_{k,0} + \frac{2\kappa_k}{G_k}\ln\left[\frac{2\kappa_k - G_k h_{k,t}}{2\kappa_k - G_k h_{k,0}}\right] = -G_k\Delta t, \tag{3.2}$$

or

$$h_{k,t} = h_{k,0} + \frac{2\kappa_k - G_k h_{k,0}}{G_k}\left\{1 - \exp\left[-\frac{G_k}{2\kappa_k}(G_k\Delta t + h_{k,t} - h_{k,0})\right]\right\}. \tag{3.3}$$

If $G_k = 0$, (3.1) can be integrated analytically to give an explicit expression for $h_{k,t}$:

$$h_{k,t} = \sqrt{h_{k,0}^2 + 4\kappa_k \Delta t}. \tag{3.4}$$

Eq. (3.2) or (3.3) must be solved iteratively. The solution to (3.3) can be found to at least 10 significant digits within 4 or 5 iterations of Newton's method (for a sufficiently small error the number of digits of accuracy doubles with each iteration) when the initial guess is taken as

$$h_{k,t}^0 = h_{k,0} + min\left[\sqrt{4\kappa_k\Delta t}, \left(\frac{2\kappa_k}{h_{k,0}} - G_k\right)min\left(\Delta t, \frac{h_{k,0}}{G_k}\right)\right], \text{ or} \tag{3.5}$$

$$F_k^0 = \Delta\rho\, min\left[\sqrt{\kappa_k/\Delta t}, \left(\frac{\kappa_k}{h_{k,0}} - \frac{G_k}{2}\right)min\left(1, \frac{h_{k,0}}{\Delta t G_k}\right)\right] + \frac{\Delta\rho G_k}{2}, \tag{3.6}$$

and subsequent iterations are

$$h_{k,t}^{n+1} = h_{k,0} + h_{k,0}\left(\frac{2\kappa_k}{G_k h_{k,0}} - 1\right)\left\{1 + \frac{\dfrac{G_k h_{k,t}^n}{2\kappa_k}}{1 - \dfrac{G_k h_{k,0}}{2\kappa_k} - \exp\left[\dfrac{G_k}{2\kappa_k}(G_k\Delta t + h_{k,t}^n - h_{k,0})\right]}\right\}. \tag{3.7}$$

The buoyancy flux implied by (3.7) is

$$\frac{F_k^{n+1}}{\Delta\rho} = \frac{h_{k,t}^{n+1} - h_{k,0}}{2\Delta t} + \frac{G_k}{2} \tag{3.8}$$

$$= \frac{G_k}{2} + \frac{h_{k,0}}{2\Delta t}\left(\frac{2\kappa_k}{G_k h_{k,0}} - 1\right)\left\{1 + \frac{\dfrac{G_k h_{k,t}^n}{2\kappa_k}}{1 - \dfrac{G_k h_{k,0}}{2\kappa_k} - \exp\left[\dfrac{G_k}{2\kappa_k}(G_k\Delta t + h_{k,t}^n - h_{k,0})\right]}\right\}$$

$$= \frac{G_k}{2} + \frac{\kappa_k}{h_{k,0}}\left(1 - \frac{G_k h_{k,0}}{2\kappa_k}\right)\left\{\frac{\dfrac{G_k h_{k,0}}{2\kappa_k} + \dfrac{h_{k,0}}{G_k\Delta t}\left[\exp\left(\dfrac{G_k F_k^n\Delta t}{\Delta\rho\,\kappa_k}\right) - 1 - \dfrac{G_k F_k^n\Delta t}{\Delta\rho\,\kappa_k}\right]}{\dfrac{G_k h_{k,0}}{2\kappa_k} + \exp\left(\dfrac{G_k F_k^n\Delta t}{\Delta\rho\,\kappa_k}\right) - 1}\right\}$$

Even a single iteration of (3.7) gives an excellent estimate of the exact flux if the first guess is qualitatively reasonable, as is the case with (3.5).

It is necessary to use a first guess like (3.6), rather than the just the flux from the previous time step, because that guess must be within the radius of convergence of the iteration given by (3.7). If another estimate of the flux, F_k^{Est}, (such as the flux from the previous time step or a previous vertical iteration through the layers - since G_k may have changed) is to be used to start the

iteration, it must be constrained to be within the physically motivated (and mathematically adequate) bounds

$$F_k^0 = \begin{cases} min\left\{\dfrac{G_k\Delta\rho}{2}, max\left[F_k^{Est}, \dfrac{\Delta\rho\kappa_k}{h_{k,0}}, \Delta\rho\left(\dfrac{\kappa_k}{\Delta t G_k} - \dfrac{h_{k,0}}{2\Delta t} + \dfrac{G_k}{2}\right)\right]\right\} & h_{k,0} \geq \dfrac{2\kappa_k}{G_k} \\[2em] max\left\{\dfrac{G_k\Delta\rho}{2}, min\left[F_k^{Est}, \dfrac{\Delta\rho\kappa_k}{h_{k,0}}, \Delta\rho\sqrt{\kappa_k/\Delta t} + \dfrac{G_k\Delta\rho}{2}\right]\right\} & h_{k,0} \leq \dfrac{2\kappa_k}{G_k} \end{cases} \text{for} . \quad (3.9)$$

Algebraic approximations to the solution for one layer

The iterative estimate of the flux can be compared with several algebraic discretizations of (3.1). A forward Euler integration of (3.1) gives

$$h_{k,t}^{\text{Forward}} = h_{k,0} + \left(\frac{2\kappa_k}{h_{k,0}} - G_k\right)\Delta t, \text{ or} \quad (3.10)$$

$$F_k^{\text{Forward}} = \frac{\Delta\rho\kappa_k}{h_{k,0}}. \quad (3.11)$$

The forward Euler integration is the simplest possible time stepping scheme, and it is perfectly adequate in the limit of slow diffusive timescales that characterizes much of the volume of the ocean.

A backward Euler integration of (3.1) gives

$$h_{k,t}^{\text{Backward}} = h_{k,0} + \left(\frac{2\kappa_k}{h_{k,t}^{\text{Backward}}} - G_k\right)\Delta t, \quad (3.12)$$

which can be solved for $h_{k,t}^{\text{Backward}}$ to give

$$h_{k,t}^{\text{Backward}} = \frac{1}{2}\left\{h_{k,0} - G_k\Delta t + \left[(h_{k,0} - G_k\Delta t)^2 + 8\kappa_k\Delta t\right]^{1/2}\right\}, \quad (3.13)$$

which implies a layer buoyancy flux of

$$F_k^{\text{Backward}} = \frac{\Delta\rho}{4\Delta t}\left\{G_k\Delta t - h_{k,0} + \left[(h_{k,0} - G_k\Delta t)^2 + 8\kappa_k\Delta t\right]^{1/2}\right\}. \quad (3.14)$$

There are two ways to write a trapezoidal scheme integration of (3.1). The first is

$$h_{k,t}^{\text{Trap1}} = h_{k,0} + \left(\frac{4\kappa_k}{h_{k,t}^{\text{Trap1}} + h_{k,0}} - G_k\right)\Delta t, \quad (3.15)$$

which can be solved for $h_{k,t}^{\text{Trap1}}$ to give

$$h_{k,t}^{\text{Trap1}} = \frac{1}{2}\left\{-G_k\Delta t + [(2h_{k,0} - G_k\Delta t)^2 + 16\kappa_k\Delta t]^{1/2}\right\}, \tag{3.16}$$

and this implies a layer buoyancy flux of

$$F_k^{\text{Trap1}} = \frac{\Delta\rho}{4\Delta t}\left\{G_k\Delta t - 2h_{k,0} + [(2h_{k,0} - G_k\Delta t)^2 + 16\kappa_k\Delta t]^{1/2}\right\}. \tag{3.17}$$

The second trapezoidal scheme integration of (3.1) is

$$h_{k,t}^{\text{Trap2}} = h_{k,0} + \left(\frac{\kappa_k}{h_{k,t}^{\text{Trap2}}} + \frac{\kappa_k}{h_{k,0}} - G_k\right)\Delta t, \tag{3.18}$$

which can be solved for $h_{k,t}^{\text{Trap2}}$ to give

$$h_{k,t}^{\text{Trap2}} = \frac{1}{2}\left\{h_{k,0} + \frac{\kappa_k\Delta t}{h_{k,0}} - G_k\Delta t + \left[\left(h_{k,0} + \frac{\kappa_k\Delta t}{h_{k,0}} - G_k\Delta t\right)^2 + 4\kappa_k\Delta t\right]^{1/2}\right\}, \tag{3.19}$$

and a layer buoyancy flux of

$$F_k^{\text{Trap2}} = \frac{\Delta\rho}{4\Delta t}\left\{\frac{\kappa_k\Delta t}{h_{k,0}} + G_k\Delta t - h_{k,0} + \left[\left(h_{k,0} + \frac{\kappa_k\Delta t}{h_{k,0}} - G_k\Delta t\right)^2 + 4\kappa_k\Delta t\right]^{1/2}\right\}. \tag{3.20}$$

All four of these schemes are consistent with the continuous equation. The two trapezoidal schemes are second order accurate in time, and exhibit smaller errors for small time steps than would the forward scheme or the backward scheme, both of which are only first order accurate in time.

Comparison between the approximations to the solution for one layer

There are several asymptotic limits of the analytic solution which can be compared with these four proposed schemes. If $h_{k,0}$ and G_k are both negligibly small, $h_{k,t}$ should remain finite for a finite time step. The backwards scheme and the first trapezoidal scheme satisfy this constraint, while the forwards scheme and the second trapezoidal scheme are unbounded for excessively small $h_{k,0}$. If $G_k = 0$, the first trapezoidal scheme (3.16) exactly reproduces the analytic solution (3.4). The backwards scheme entrains too little with $G_k = 0$ - by a factor of $(1 - \sqrt{1/2})$ for infinitesimal $h_{k,0}$ and by a factor of $(\kappa_k\Delta t/h_{k,0}^2)$ for large $h_{k,0}$.

For very large time steps, $h_{k,t}$ should tend toward $(2\kappa_k/G_k)$. Only the backwards scheme satisfies this constraint. The first trapezoidal scheme tends toward $(-h_{k,0} + 4\kappa_k/G_k)$, which may be negative. The second trapezoidal scheme and the forward scheme are both unbounded, although the second trapezoidal scheme is at least guaranteed to yield positive $h_{k,t}$. The second trapezoidal scheme will not be considered further in this paper because of its unstable behavior for small values
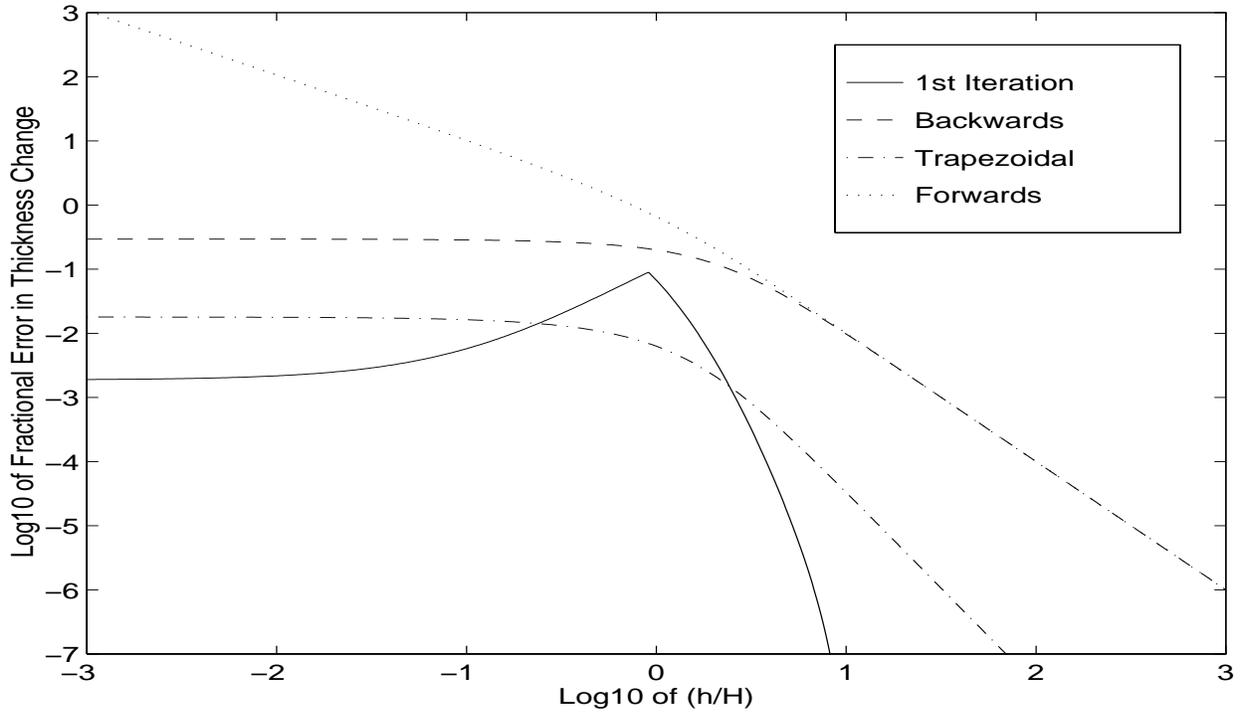
Figure 1. Fractional error of the thickness changes within one time step calculated with four schemes, relative to the flux calculated by iterating (3.8) to convergence, with $G_k/\Gamma = 0.2$. The fluxes with these four schemes are given by one iteration of (3.8) starting from (3.5), (3.14) for the backwards scheme, (3.11) for the forwards scheme, and (3.17) for the first trapezoidal scheme.

of $h_0^2/\kappa\Delta t$. The forwards scheme will be considered, but only because of its previous use in the literature (Hu, 1996a; McDougall and Dewar, 1998).

The trapezoidal schemes are superior to the backwards scheme for short time steps, while the backwards scheme is the only one of the four algebraic schemes presented above to reproduce the qualitative behavior of the exact solution in all of the relevant asymptotic limits. It is possible to construct a second order accurate scheme with two iterations of the backwards scheme that exhibits qualitatively correct behavior for all of the criteria discussed above, but this scheme is as complicated and computationally expensive as the more accurate exact iterative solution discussed above.

There are only two free parameters in (3.1) after it has been nondimensionalized by dividing $h_{k,0}$ by $H = \sqrt{\kappa_k \Delta t}$ and dividing G_k by $\Gamma = \sqrt{\kappa_k/\Delta t}$. The fractional error in the layer thickness change over one time step calculated with the various schemes relative to the exact solution is depicted in Fig. 1 and Fig. 2 for two values of G_k. For a small value of G_k (Fig. 1), all of the schemes except the forwards scheme give qualitatively accurate fluxes for all initial thicknesses. Typically $h \gg H$, and in this part of parameter space, all of the schemes are accurate, but the trapezoidal scheme and the first iteration towards the exact scheme give a very high degree of accuracy.
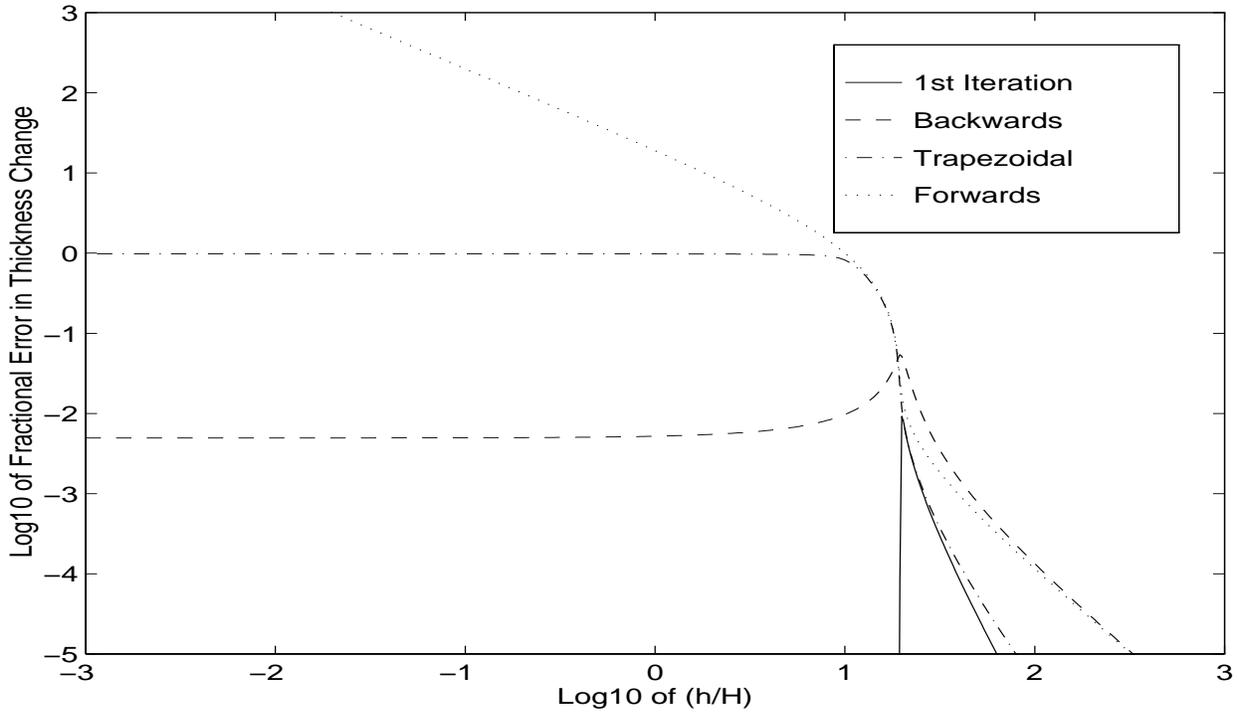
Figure 2. As in Fig. 1, but with $G_k/\Gamma = 20$. The equivalent plot with a much larger value of G_k/Γ is qualitatively similar.

With a large value of G_k (Fig. 2), all of the schemes have some problems when $h \approx G_k \Delta t$ - the first iteration towards the exact scheme gives a reasonably accurate estimate of the flux, while the backwards scheme overestimates the flux. The forwards scheme and trapezoidal scheme tend to drastically underestimate the flux and the thickness after a time step can be negative for these two schemes, as seen in Fig. 3. Reasonable behavior in the limit of large G_k is essential if the model is to be useful for simulation of strongly entraining flows, such as flow of dense water over a sill.

The two schemes among those listed above which satisfy all of the desired properties are the backwards scheme and the first iteration (or repeated iteration) towards the exact scheme starting with a reasonably accurate first guess. The backwards scheme is simpler, but the first iteration is significantly more accurate. The relative expense of the two schemes depends partially on whether it is more expensive to evaluate an exponential function or a square root, but the exact iterative scheme is generally much more complicated. Also the exact scheme requires a reasonably accurate starting guess for the iteration. Both schemes always yield positive thicknesses, both asymptote to $G_k/2$ for large G_k, and both are well behaved for small initial thicknesses.

Although it is only first order accurate in time, the backwards scheme exhibits qualitatively correct behavior in all limits, which makes this scheme attractive. If an exceedingly accurate solution to (3.1) were desired, the iterative exact scheme would be the best choice, but for use with an ocean model it is simply not reasonable to use a highly accurate but expensive scheme. The computational resources could certainly be used more efficiently to minimize truncation errors associ-
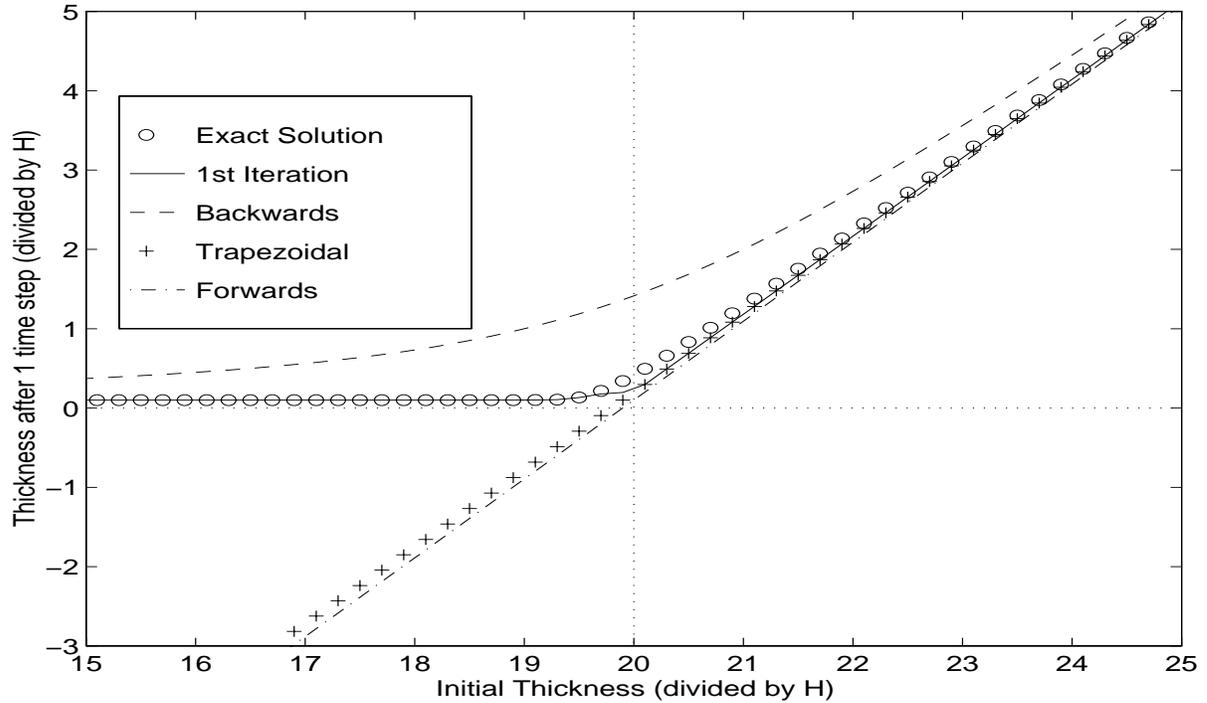
Figure 3. Thickness after one time step with $G_k/\Gamma = 20$. The schemes are the same as are depicted in Fig. 1 and Fig. 2.

ated with resolution or the parameterization of other physical processes. Still, the fact that first iteration towards the exact scheme gives qualitatively correct approximations to the solution to (3.1) in all limits and is often significantly more accurate than any of the algebraic discretizations may make this first iteration a viable scheme for consideration with ocean models. In the next section the backwards scheme and the first iteration are examined for use in simultaneously solving the set of equations (3.1) for many layers.

4. Integration of the Diffusion Equation for Multiple Layers

For any of the schemes presented in §3 except the forward scheme, the diffusive buoyancy flux in each layer depends nonlinearly on the fluxes in both of its neighbors. This prevents these coupled equations from being solved simply with standard techniques. Also, the boundary conditions are somewhat peculiar with density coordinates because the coordinates diffuse out of the domain and the density at which the boundary conditions must be applied changes over time. An effective method of handling these complications is described in this section.

Boundary conditions

Buoyancy flux boundary conditions are applied at the topmost and bottommost interfaces. In order to conserve volume (or mass if the thicknesses are reinterpreted as pressure differences

between the interfaces above and below a layer) and the density of the topmost or bottommost layers, there can be no buoyancy flux convergence at these outermost interfaces, so the buoyancy flux within the topmost or bottommost layer must equal the buoyancy flux boundary condition. (A mass source or sink boundary condition due to evaporation and precipitation or freezing and melting at the bottom of sea ice can be applied instead fairly easily.) At interior interfaces, all layers entrain fluid from their neighboring layers at a rate proportional to the buoyancy flux within that layer. The net flux of fluid across an interface is simply given by $(F_k - F_{k-1})/\Delta\rho_{k-1/2}$, so the maximum buoyancy flux that can occur within layer k for a timestep while still leaving at least a thickness ε within each of the overlying layers is given by

$$F_k^{\text{max},\,a} = F_{k-1}^{\text{max},\,a} + \frac{\Delta\rho_{k-1/2}}{\Delta t}\sum_{j=1}^{k-1}(h_j-\varepsilon) = F_1 + \frac{1}{\Delta t}\sum_{i=2}^{k}\Delta\rho_{i-1/2}\sum_{j=1}^{i-1}(h_j-\varepsilon),\qquad(4.1)$$

with $F_1^{\text{max},\,a} = F_1$ from the surface flux boundary condition. The schemes presented here all work perfectly well with $\varepsilon = 0$, but it may be useful (for example in calculating the vertical viscosity or the Coriolis terms using a potential vorticity conserving discretization) to use a very small positive ε. Hallberg and Rhines (1996) use $\varepsilon = 10^{-10}$ m, and the same, absurdly small value is used in the calculations here. The value of ε should be taken to be sufficiently small that any physically reasonable amount of diffusion is not hindered. Similarly, the maximum buoyancy flux that can occur within a timestep while leaving at least a thickness ε within each of the layers below is

$$F_k^{\text{max},\,b} = F_{k+1}^{\text{max},\,b} + \frac{\Delta\rho_{k+1/2}}{\Delta t}\sum_{j=k+1}^{N}(h_j-\varepsilon) = F_N + \frac{1}{\Delta t}\sum_{i=k}^{N-1}\Delta\rho_{i+1/2}\sum_{j=i+1}^{N}(h_j-\varepsilon)\qquad(4.2)$$

with $F_N^{\text{max},\,b} = F_N$ implementing the bottom flux boundary condition. The maximum buoyancy flux for each layer (including the top and bottom layers) is

$$F_k^{\text{max}} = min(F_k^{\text{max},\,a}, F_k^{\text{max},\,b}).\qquad(4.3)$$

There is a possibility that $F_1^{\text{max},\,b} < F_1$ or that $\,_N^{\text{max},\,a} < F_N$, in which case the buoyancy flux at the top or bottom must be modified; in this case the surface or bottom buoyancy forcing can not be accommodated with the given resolution in density space because all of the fluid is already in the lightest or densest layer.

Interior Solutions

The exact solution to the set of equations given by any of the schemes from §3, with appropriately implemented boundary conditions can be found iteratively. For example, if the backwards Euler integration scheme is adopted, an initial refinement of the flux in layer k, given the previous guesses for the fluxes in all of the layers is

$$F_k^{n,0} = min(F_k^{\text{Backward}}(G_k^{n-1}), F_k^{\text{max}}) \qquad , \qquad (4.4)$$

$$= min\left(\frac{\Delta\rho_k}{4\gamma_k\Delta t}\left\{G_k^{n-1}\Delta t - h_{k,0} + [(h_{k,0} - G_k^{n-1}\Delta t)^2 + 8\gamma_k\kappa_k\Delta t]^{1/2}\right\}, F_k^{\text{max}}\right)$$

where n is the iteration number,

$$G_k^{n-1} = \frac{F_{k-1}^{n,0}}{\Delta\rho_{k-1/2}} + \frac{F_{k+1}^{n-1}}{\Delta\rho_{k+1/2}}, \text{ and}$$

$$\gamma_k = \frac{1}{2}\left(\frac{\Delta\rho_k}{\Delta\rho_{k-1/2}} + \frac{\Delta\rho_k}{\Delta\rho_{k+1/2}}\right). \qquad (4.5)$$

The sensitivity of this equation to changes in the fluxes of the adjacent layers is given by

$$\frac{\partial F_k^n}{\partial G_k} = \left(\begin{array}{ll} \dfrac{\Delta\rho_k}{4\gamma_k}\left\{1 + \dfrac{G_k\Delta t - h_{k,0}}{[(h_{k,0} - G_k\Delta t)^2 + 8\gamma_k\kappa_k\Delta t]^{1/2}}\right\} & \text{for } (F_k^{n,0} < F_k^{\text{max}}) \\ 0 & \text{for } (F_k^{n,0} \geq F_k^{\text{max}}) \end{array}\right). \qquad (4.6)$$

The exact iterative scheme of the previous section, (3.8), can be used with one iteration of each layer equation per iteration through all the layers, subjecting each previous estimate to limits to insure that it is qualitatively reasonable with the updated values of G_k. The algebra is much more complicated with that scheme, but the derivation of the equivalent expression is straightforward, so it will be omitted here. Linearizing around the estimated fluxes from (4.4) gives a set of equations for the F_k^n based on Newton's method

$$F_k^n = min\left[F_k^{n,0} + \frac{\partial F_k^n}{\partial G_k}\left(\frac{F_{k+1}^n - F_{k+1}^{n-1}}{\Delta\rho_{k+1/2}} + \frac{F_{k-1}^n - F_{k-1}^{n,0}}{\Delta\rho_{k-1/2}}\right), F_k^{\text{max}}\right] \qquad (4.7)$$

with the boundary conditions $F_1^n = F_1^{\text{max}}$ and $F_N^n = F_N^{\text{max}}$. This tridiagonal set of equations is straightforward to solve. The logical constraints in (4.6) and (4.7) are not the formidable complications that they might seem to be, because if any layer k has a flux of F_k^{max}, either all of the layers above or all of the layers below have a flux F_j^{max} for layer j. A reasonable starting guess of the fluxes for use with the first iteration is

$$F_k^{0,0} = min(\Delta\rho_k\sqrt{\kappa_k/\gamma_k\Delta t}, \Delta\rho_k\kappa_k/h_{k,0}, F_k^{\text{max}}). \qquad (4.8)$$

This vertical iteration usually converges rapidly to the exact solution of the set of equations; there is an appreciable error in the first iteration (although the solution is not qualitatively wrong) only when $h_{k\pm1,0} \approx min(\sqrt{\kappa_k\Delta t}, \kappa_k\Delta t/h_{k,0})$ in several adjacent interior layers, at which value there is a transition between the large and small thickness asymptotic limits. The fluxes in much thicker layers are largely independent of the fluxes in their neighbors, while the linearization in
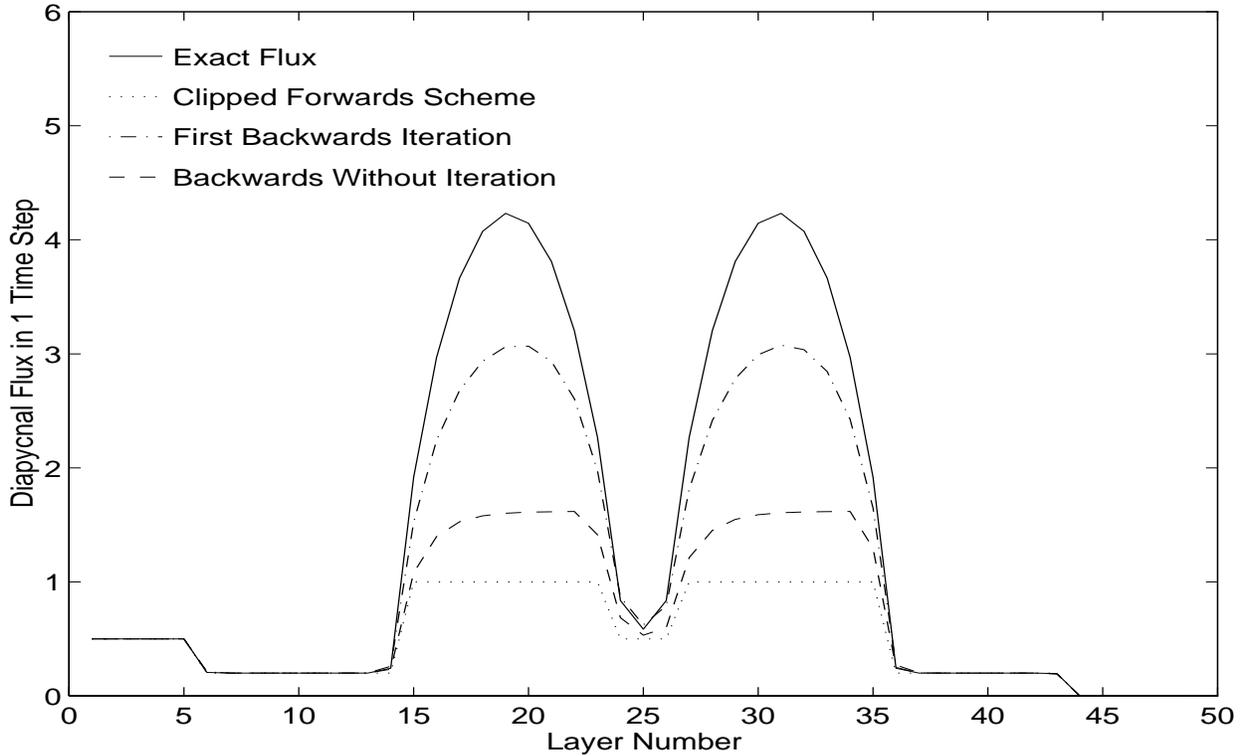
Figure 4. Diapycnal fluxes in one time step, in units of $(\Delta\rho\sqrt{\kappa\Delta t})$ for various schemes. The clipped forwards scheme is the minimum of the flux from a forwards Euler calculation and $(\Delta\rho\sqrt{\kappa\Delta t})$. The two backwards schemes differ only in the lack of the iterative correction as described by (4.7). The exact flux is found by iterating the Newton's method scheme to convergence. The diffusivities and density differences between layers are uniform. Layers 1-5, 15-23, 27-35 and 45-50 are initially essentially massless ($10^{-8}\sqrt{\kappa\Delta t}$ or $10^{-12}\sqrt{\kappa\Delta t}$ - it makes no difference); layers 6-14 and 36-44 have thickness $(5\sqrt{\kappa\Delta t})$, while layers 24-26 have thickness $(2\sqrt{\kappa\Delta t})$. There is an insulating bottom boundary condition and a downward surface flux of $(0.5\Delta\rho\sqrt{\kappa\Delta t})$.

(4.7) is an excellent approximation for thinner layers. When the layers have approximately this intermediate thickness, the backwards scheme converges more rapidly than does the exact iterative scheme because $\partial F/\partial G$ changes less abruptly with changing G with the backwards scheme.

An example of the fluxes generated by various schemes with several density fronts in the middle of a fluid is given in Fig. 4. The initial density profile has two arbitrarily sharp and well resolved interior density fronts. Massless layers are included at the top and bottom of the profile to demonstrate that the boundary conditions are correctly implemented with all the schemes. The forwards Euler fluxes shown in Fig. 4 are truncated at a value of $(\Delta\rho\sqrt{\kappa\Delta t})$. This is the maximum truncation value for which the neighboring layer will not be depleted with constant diffusivities and density differences between layers. In practice a smaller truncation flux would have to be used if the diapycnal diffusivity has vertical variations. Even with this large truncation flux, the forwards Euler flux dramatically underpredicts the fluxes across the interior fronts. The backwards scheme

without iteration similarly underpredicts the fluxes through the front, but at least in real simulations this scheme could be implemented with the same accuracy seen in this simple demonstration. The fluxes through the fronts are dramatically improved by even a single iteration of the form given by (4.7) for either the backwards Euler scheme or the scheme based on Newton's method. Subsequent iterations rapidly reduce the errors further. (The two schemes differ both with the first iteration and at convergence, but by relatively small amount; in Fig. 4 this difference would only be about $0.1(\Delta\rho\sqrt{\kappa\Delta t})$.) If there are strongly varying diffusivities with depth, the relative improvement of the iterative schemes can be much greater than depicted here.

The computational expense of various schemes are shown in Table 1. These statistics are only for calculations of the layer fluxes which will yield positive definite layer thicknesses. The computational requirements for implicit vertical advection of two velocities are included for comparison. All of these schemes scale linearly with the number of layers, and enough layers are used that the slightly different treatment of the uppermost and bottommost interior layers is not significant. Since the entire calculation of diapycnal fluxes and diapycnal advection is typically on the order of 10% of the total CPU time involved with the baroclinic portion of an ocean model simulation, replacing a crudely limited forwards Euler scheme with a single iteration of the backwards scheme will increase the overall model run time by about 10-12%. Multiple iterations with either scheme are probably prohibitively expensive for common use, while the backwards scheme without iteration only increases the total run time by 3-6%. On the other hand, for studies where accurate portrayal of diapycnal diffusion is important or with significant variations of diapycnal diffusivity, such as simulation of an entraining density current, the iterative schemes provide excellent solutions at modest expense.

Scheme \ Computer	SGI Indigo	Cray T90
Forwards Euler with positive definite limitations	1	1
Backwards Scheme without Iteration	3.3	2.0
1 Iteration with Backwards Scheme	4.8	5.0
Additional Iterations with Backwards Scheme	3.3	3.6
1 Iteration with Newton Method Scheme	7.5	8.4
Additional Iterations with Newton Method Scheme	5.9	7.1
(Vertical advection of two velocity components.)	2.8	2.5
TABLE 1. Relative CPU time requirements of various schemes on two computers.		

5. Richardson Number Dependent Entrainment

There are several places in the ocean where velocity shears that might be resolvable by an ocean GCM drive significant turbulent mixing. Strong turbulent mixing is important for both the

mass and momentum budgets of the equatorial undercurrents (Jones, 1973; Wacongne, 1989; Pedlosky, 1996). While there is strong observational evidence that high-frequency, small scale shears are as important as the resolvable scale shears in driving the mixing (Peters et al., 1995), there has been considerable success with parameterizations based on the resolved Richardson number due to shears with vertical scales of tens of meters (Pacanowski and Philander, 1981; Yu and Schopf, 1997). Essentially these parameterizations are able to reproduce the observation that the resolvable Richardson numbers are never too small, and just enough mixing occurs to keep the Richardson numbers at or above some threshold value, even if the variability of the mixing or its exact cause are not captured. The gravity currents generated by the overflow of dense waters from marginal seas such as the Mediterranean and Nordic seas exhibit intense entrainment, doubling or even quadrupling their volume flux within a few days (Price and Baringer, 1994). This entrainment is absolutely critical in determining the watermass properties that fill the open ocean, but since most of the entrainment occurs very vigorously across extremely sharp density gradients it is difficult to simulate this process accurately. This section presents a Richardson number dependent mixing scheme which will be shown in the next section to give reasonable entrainment in a simple simulation of a gravity current.

Price and Baringer (1994) successfully model the entrainment into a gravity current using the Richardson number dependent entrainment parameterization which Turner (1986) has developed based on laboratory simulations. According to Turner (1986), the entrainment rate of a gravity current is well parameterized by

$$w_E = \begin{cases} \Delta U \dfrac{0.08 - 0.1Ri_B}{1 + 5Ri_B} & Ri_B < 0.8 \\ 0 & Ri_B \geq 0.8 \end{cases}, \tag{5.1}$$

where ΔU is the magnitude of the velocity difference between the gravity current and the environment and the bulk Richardson number is given by

$$Ri_B = \frac{g\Delta\rho h}{\rho(\Delta U)^2}. \tag{5.2}$$

In discrete isopycnal layers the appropriate definition of the layer Richardson number is

$$Ri_k = \frac{2\Delta\rho_{k-1/2}\Delta\rho_{k+1/2}gh_k}{\rho_k(\Delta\rho_{k+1/2}\|\vec{u}_k - \vec{u}_{k-1}\|^2 + \Delta\rho_{k-1/2}\|\vec{u}_k - \vec{u}_{k+1}\|^2)}. \tag{5.3}$$

Eq. (5.3) is obtained by comparing the changes in kinetic and potential energy when a layer entrains a small amount of fluid and by requiring that these changes balance when $Ri_k = 1$. With this formula for the layer Richardson number, Turner's parameterization, (5.1), can be used without modification. To maintain the density of the layer in question, the entrainment into layer **k** from above and below must be related by $w_k^+ \Delta\rho_{k+1/2} = w_k^- \Delta\rho_{k-1/2}$. Since (5.1) is essentially a

parameterization of entrainment from above into a layer with a density that is much closer to the density of the existing bottom boundary layer than to the interior density, the final parametrization should agree with (5.1) when $\Delta\rho_{k+1/2} \ll \Delta\rho_{k-1/2}$ and $\Delta\rho_{k+1/2}\|\grave{u}_k - \grave{u}_{k-1}\|^2 \gg \Delta\rho_{k-1/2}\|\grave{u}_k - \grave{u}_{k+1}\|^2$. With this constraint, a consistent estimate of $\Delta\rho\Delta U$ across a layer is given by

$$
\Delta\rho_{k+1/2}\Delta U_k^+ = \Delta\rho_{k-1/2}\Delta U_k^- = \frac{\Delta\rho_{k-1/2} + \Delta\rho_{k+1/2}}{2}\left(\frac{g\Delta\rho_k h_k}{\rho_k Ri_k}\right)^{1/2}
$$

$$
= \left[\frac{(\Delta\rho_{k-1/2} + \Delta\rho_{k+1/2})^3}{4\Delta\rho_{k-1/2}\Delta\rho_{k+1/2}}(\Delta\rho_{k+1/2}\|\grave{u}_k - \grave{u}_{k-1}\|^2 + \Delta\rho_{k-1/2}\|\grave{u}_k - \grave{u}_{k+1}\|^2)\right]^{1/2}
$$

. (5.4)

When the density differences between layers are equal, (5.4) is simply

$$
\Delta U_k = [2(\|\grave{u}_k - \grave{u}_{k-1}\|^2 + \|\grave{u}_k - \grave{u}_{k+1}\|^2)]^{1/2} \approx \|\grave{u}_{k+1} - \grave{u}_{k-1}\|, \tag{5.5}
$$

where the final, approximate expression holds when the velocity of layer k is the average of the velocities of its neighbors. So the equivalent expression for discrete layers to Turner's parameterization for Richardson number dependent entrainment becomes

$$
w_k^{\pm} = \begin{cases} \Delta U^{\pm}\dfrac{0.08 - 0.1 Ri_k}{1 + 5Ri_k} & Ri_k < 0.8 \\[2mm] 0 & Ri_k \geq 0.8 \end{cases}, \tag{5.6}
$$

where $_k^{\pm}$ is entrainment from layer $k \pm 1$ into layer k, and $\Delta U^{\pm}$ and Ri_k are defined in (5.4) and (5.3). The entrainment rates given by (5.6) are most appropriately interpreted as the *net* entrainment of a layer, not the total entrainment; this interpretation gives results which are consistent with the original Turner parameterization when there are multiple thin layers separating the entraining gravity current from the interior.

Ideally both the velocities and the layer thickness in (5.3) and (5.4) would be treated implicitly, and a sufficient number of vertical iterations could be used to determine the exact solution to the set of equations found by substituting the entrainment rates given by (5.6) into (3.1). But this approach would be too time consuming for practical use - in order to guarantee convergence the number of iterations would have to be on the order of the number of layers. Instead an approximate estimate of the net velocity differences after a time step will be used here with a scheme that is implicit in the layer thickness.

The velocity differences between layers before the entrainment may be quite different from the differences afterwards, especially for thin layers. For example, if vertical viscosity with coefficient ν is applied before diapycnal diffusion, adjacent layers that are much thinner than $\sqrt{\nu\Delta t}$ will have approximately the same velocities. (Hallberg and Rhines (1996) use an upwind-biased verti-

cal viscosity to solve the difficulties associated with calculating the Montgomery potential gradient near the point where an isopycnal intersects the sloping bottom.) A reasonable estimate for the final velocity differences might be the velocities that each layer would have if it entrained enough to have at least some minimum thickness, say $h_{min} = \sqrt{\nu \Delta t}$ or $\sqrt{\kappa \Delta t}$, if this fluid were not in turn entrained by neighboring layers. (The exact value of h_{min} is relatively unimportant in most instances.) These estimated velocities can be calculated implicitly with a tridiagonal set of equations:

$$(u, v)_k^{est} = \frac{h_k^0 (u, v)_k^0 + H_k^e \left(\dfrac{\Delta \rho_{k-1/2} (u, v)_{k+1}^{est} + \Delta \rho_{k+1/2} (u, v)_{k-1}^{est}}{\Delta \rho_{k-1/2} + \Delta \rho_{k+1/2}} \right)}{h_k^0 + H_k^e}, \tag{5.7}$$

where

$$H_k^e = min \left\{ \begin{array}{l} max[(h_{min} - h_k^0), 0], \\[2ex] min \left[\left(1 + \dfrac{\Delta \rho_{k+1/2}}{\Delta \rho_{k-1/2}} \right) \displaystyle\sum_{j=k+1}^{N} (h_j - \varepsilon), \left(1 + \dfrac{\Delta \rho_{k-1/2}}{\Delta \rho_{k+1/2}} \right) \displaystyle\sum_{j=1}^{k-1} (h_j - \varepsilon) \right] \end{array} \right\} \tag{5.8}$$

is an estimated entrainment rate with limitations to prevent entrainment of nonexistent fluid. Essentially this step is only necessary to prevent extremely large or small shears in small amounts of fluid from having an excessively large influence on the evolution of a simulation. The velocities of sufficiently thick layers are unaltered by this approach, while velocity shears are roughly homogenized over a vertical distance over which the background viscosity or diffusivity might be expected to work within a time step.

The layer Richardson numbers are proportional to the layer thicknesses, so it is straightforward to write an easily solvable time integration scheme for (5.6) that is implicit in the layer thickness and explicit in the layer velocities. Defining

$$\eta_k \equiv \frac{h_k}{Ri_k} = \rho_k \frac{(\Delta \rho_{k+1/2} \| \grave{u}_k - \grave{u}_{k-1} \|^2 + \Delta \rho_{k-1/2} \| \grave{u}_k - \grave{u}_{k+1} \|^2)}{2g \Delta \rho_{k+1/2} \Delta \rho_{k-1/2}} \tag{5.9}$$

to be the layer thickness at which the Richardson number would be 1 and using the entrainment defined by (5.6), the equation for the layer thickness after a time step of turbulent mixing is

$$h_k^{Turb} = \left\{ \begin{array}{ll} h_k^n + \Delta t (\Delta U_k^{est+} + \Delta U_k^{est-}) \dfrac{0.08 \eta_k - 0.1 h_k^{Turb}}{\eta_k + 5 h_k^{Turb}} & h_k^n < 0.8 \eta_k \\[3ex] 0.8 \eta_k & h_k^n \geq 0.8 \eta_k \end{array} \right. . \tag{5.10}$$

The choice that the layer should detrain down to the critical thickness when it is thicker than this thickness is because the final flux will be taken as the maximum of this turbulent flux and the dif-

fusive flux - this choice limits the amount of net detrainment that a layer can experience due to turbulence in neighboring layers. The $h_k^n < 0.8\eta_k$ branch of (5.10) can easily be solved for h_k^{Turb}, giving

$$h_k^{\text{Turb}} = 0.5h_k^n - 0.1\eta_k - 0.01\Delta t(\Delta U_k^{est+} + \Delta U_k^{est-}) \qquad .$$

$$+ \left\{ [0.5h_k^n - 0.1\eta_k - 0.01\Delta t(\Delta U_k^{est+} + \Delta U_k^{est-})]^2 \right.$$

$$\left. + [0.2h_k^n + 0.016\Delta t(\Delta U_k^{est+} + \Delta U_k^{est-})]\eta_k \right\}^{\frac{1}{2}}$$

(5.11)

So when $h_k^n < 0.8\eta_k$, the diffusive buoyancy flux is given by

$$F_k^{\text{Turb}} = \frac{\Delta\rho_k}{2\gamma_k}\left(G_k - 0.5\frac{h_k^n}{\Delta t} - 0.1\frac{\eta_k}{\Delta t} - 0.01(\Delta U_k^{est+} + \Delta U_k^{est-}) \right.$$

$$+ \left\{ \left[0.5\frac{h_k^n}{\Delta t} - 0.1\frac{\eta_k}{\Delta t} - 0.01(\Delta U_k^{est+} + \Delta U_k^{est-}) \right]^2 \right.$$

$$\left.\left. + \left[0.2\frac{h_k^n}{\Delta t} + 0.016(\Delta U_k^{est+} + \Delta U_k^{est-}) \right]\frac{\eta_k}{\Delta t} \right\}^{\frac{1}{2}} \right)$$

(5.12)

which is always greater than $G_k\Delta\rho_k/2\gamma_k$. (Recall that γ_k, defined by (4.5), is a ratio of density differences that is 1 for equal density differences.) When $h_k^n \geq 0.8\eta_k$

$$F_k^{\text{Turb}} = \frac{\Delta\rho_k}{2\gamma_k}\left(G_k - \frac{h_k^n - 0.8\eta_k}{\Delta t} \right).$$

(5.13)

In both limits

$$\frac{\partial F_k^{\text{Turb}}}{\partial G_k} = \frac{\Delta\rho_k}{2\gamma_k},$$

(5.14)

which is the same as the large G_k limit of its diffusive counterpart. The final buoyancy flux through a layer is then given by

$$F_k = min(F_k^{\text{max}}, max(F_k^{\text{Diffusive}}, F_k^{\text{Turb}})),$$

(5.15)

where F_k^{max} is defined by (4.3) and $F_k^{\text{Diffusive}}$ is defined by (4.4). The entrainment parameterization given by (5.15) is depicted in Fig. 5 for one qualitatively illustrative case. The partial derivative F_k with respect to G_k is chosen to correspond with the definition of F_k:
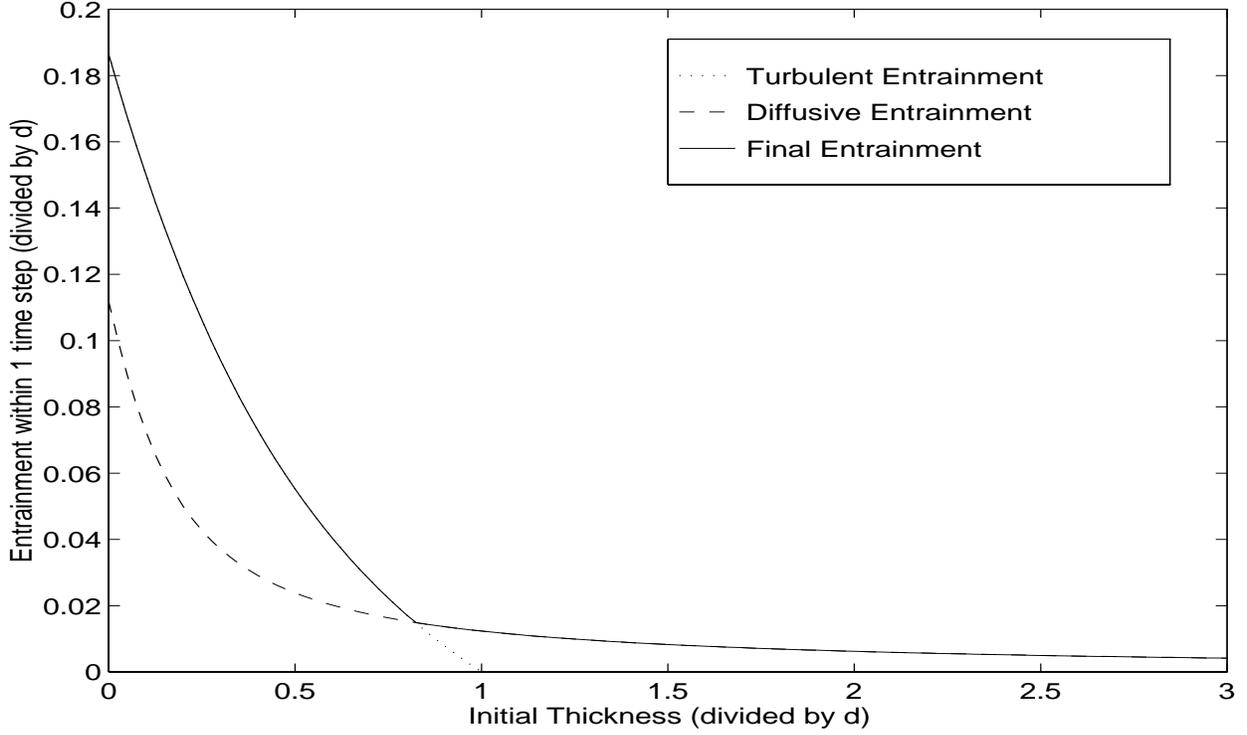
Figure 5. Entrainment within a time step as parameterized by (5.15) as a function of the initial
layer thickness, normalized by $d = 0.8\eta_k$, the critical thickness for turbulent entrainment.
This example has $G_k=0$, $\Delta U_k^{est}\Delta t = d$, and $\kappa_k \Delta t = 0.001d$.

$$\frac{\partial F_k}{\partial G_k} = \begin{pmatrix} \partial F_k^{\text{Turb}}/\partial G_k & F_k^{\text{Diffusive}} < F_k^{\text{Turb}}, F_k^{\max} > max(F_k^{\text{Diffusive}}, F_k^{\text{Turb}}) \\ \partial F_k^{\text{Diffusive}}/\partial G_k & \text{for} \quad F_k^{\text{Diffusive}} > F_k^{\text{Turb}}, F_k^{\max} > max(F_k^{\text{Diffusive}}, F_k^{\text{Turb}}) \\ 0 & F_k^{\max} \leq max(F_k^{\text{Diffusive}}, F_k^{\text{Turb}}) \end{pmatrix}, \quad (5.16)$$

These definitions are then used with the vertically iterative Newton's method based scheme
described in (4.7).

       The scheme described here is just one particular Richardson number dependent scheme.
Any implicit scheme for which both the buoyancy flux within a layer and the derivative of that flux
with respect to the fluxes in neighboring layers can be found efficiently could be used equally well
in isopycnal coordinate models with the proposed framework. Many proposed parameterizations
of Richardson number dependent mixing, however, would involve solving a quartic equation (Pac-
anowski and Philander, 1981) or a higher order polynomial without an analytic solution. Yu and
Schopf (1997) have compared a number of Richardson number dependent mixing schemes, and
find that the exact parameterization at small Richardson numbers has very little impact on the flow
in the equatorial Pacific, provided that mixing is large at small Richardson number and that there
is an abrupt change in the mixing rates near an appropriate critical Richardson number. The current
scheme satisfies this condition.

6. An Entraining Gravity Current

The recent DYNAMO ocean model intercomparison project found that while geopotential coordinate models and sigma coordinate models exhibited excessive entrainment in the denser portions of the East Greenland current, downstream of Denmark Strait, an isopycnal coordinate ocean model exhibited dramatically insufficient entrainment (DYNAMO Group, 1997). This weak entrainment leads to deep flow around the tip of Greenland that is both much denser and with a much smaller volume flux than in the real world, despite a reasonable flow through Denmark Strait. Over time, this and a similar lack of entrainment in other dense water flows over sills could lead to substantial deviations of the deeper watermass properties throughout the world from those observed.

The value of the new time integration scheme is demonstrated with a qualitative simulation of an entraining gravity current. The parameters chosen here are similar to those used by Price and Baringer (1994) in their streamtube model of the Mediterranean water overflow. A single column model is used, and it is assumed to move along with the flow, while all horizontal effects are neglected. The interface between each layer is assumed to be parallel to the specified bottom slope, which increases linearly with time over 1/2 day up to a value of 0.01, while the upper layer is at rest, so the horizontal pressure gradients increase linearly with density. Initially there is a 100 m thick layer of fluid resting on the bottom that is 2 kg m^{-3} denser than the interior fluid. The fluid accelerates from rest subject to Coriolis acceleration with $f = 7.29\times10^{-5}$ s^{-1}, bottom drag due to a near-bottom viscosity of 2×10^{-2} m^2 s^{-1}, and an interior background vertical viscosity of 10^{-4} m^2 s^{-1} in addition to turbulent Prandtl number 1 entrainment. Entrainment is parameterized by (5.12) and (5.13) or a background diapycnal diffusion of 10^{-4} m^2 s^{-1} (whichever is greater). (So in this simulation the Prandtl number is always between 2 for entrainment due to the background diffusion and 1 for turbulent entrainment.) A time step of 1 hour, a reasonable value for a moderately high resolution ocean simulation, is used in all of these experiments except in one very high resolution case, which is essentially converged in both vertical and temporal resolution. The results from the single column model are qualitatively similar to three-dimensional tests. The single column demonstration is presented here because it isolates the effects of diapycnal diffusion and the Richardson number entrainment from more complicated spatially varying processes.

As the fluid accelerates down the slope, there is initially intense entrainment, but the velocities are arrested by the Coriolis force, and subsequent bursts of entrainment occur at about the same phase of the inertial oscillation. This rapid adjustment is seen quite clearly in an example with 50 layers using the vertically iterative implicit entrainment scheme described in the previous two sections (Fig. 6a). Almost all of the entrainment occurs within the first day or two, both in this example and in entraining gravity currents in the real ocean (Price and Baringer, 1994). 50 layers is much more resolution than would be reasonable in a simulation of the large scale ocean circula-
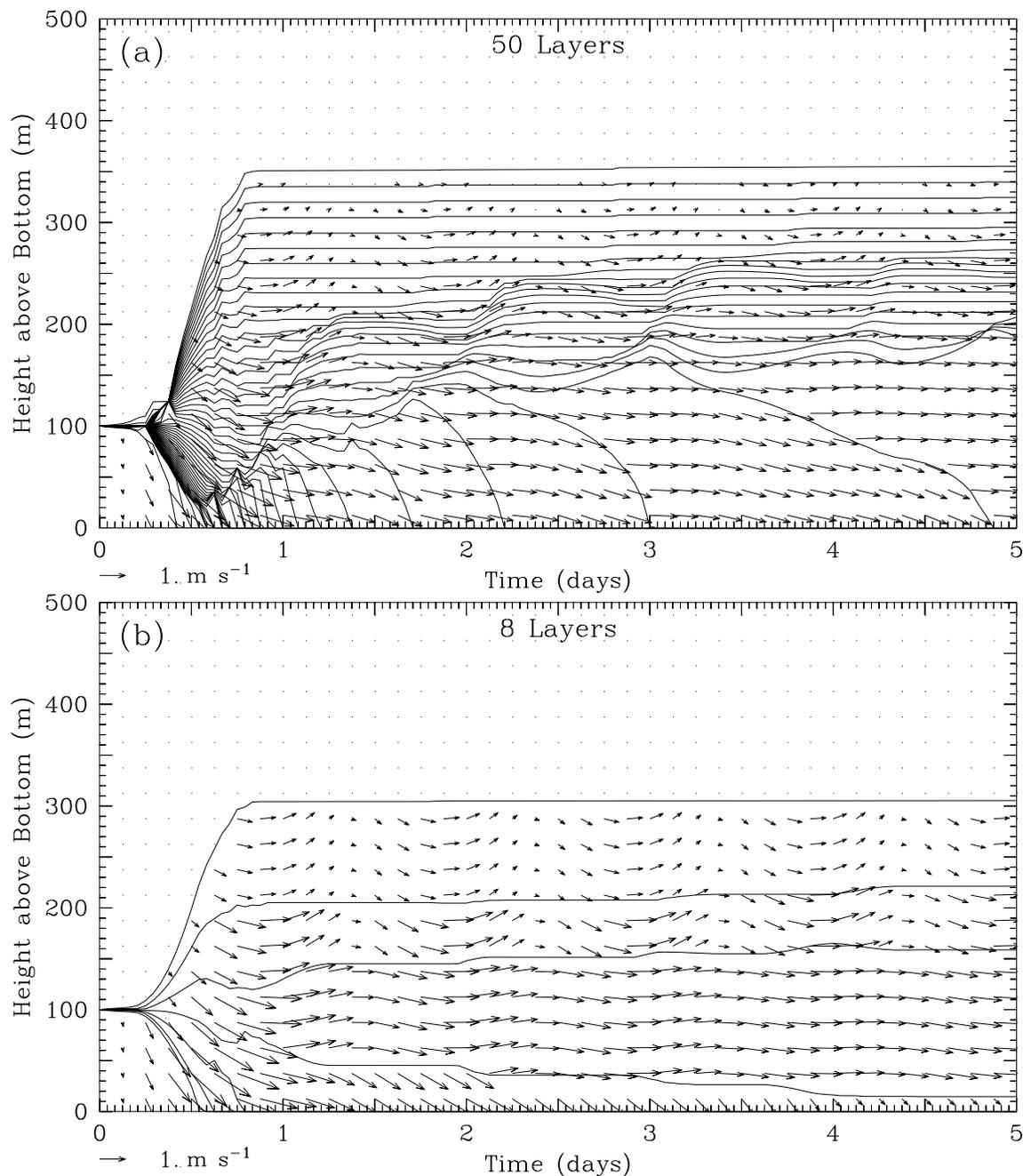
Figure 6. Isopycnal depths and velocities (along-channel to the right, upslope upwards) as a
function of time and depth for an entraining gravity current on a slope that increases up to
1% over the first half day, initially with 50 layers (a) or 8 layers (b). The backwards scheme
is used for each layer with 1 full iteration through the layers to calculate the entrainment.
The physical system is identical in the two figures, and is described fully in the text.

tion, but it is not unreasonable to expect that there would be at least 6 layers between the density
at which the Mediterranean water flows through the Strait of Gibraltar and the ambient Atlantic
water. With only 8 layers, the results are remarkably similar to those from the 50 layer simulation

of the same physical process (Fig. 6b). While some details, such as the later inertial oscillation driven entrainment in the middle of the stratified transition between the bottom boundary layer and the interior, are muted with the coarse resolution in density, the most important aspects of the higher resolution version have been captured to the extent that the vertical resolution allows. The results from these demonstrations of the implicit, vertically iterative Richardson number entrainment scheme are similar to those reported by Price and Baringer (1994) both for a specially developed streamtube model and to the observed downstream evolution of the Mediterranean water plume.

There are a few instances in Fig. 6a where a layer becomes quite thin. These points are a result of only using 1 vertical iteration; with 4 iterations they do not occur anywhere in this test. When not enough iterations are used for the solution to converge, it is necessary to limit the fluxes to guarantee that there will be no negative thickness layers. If the estimate of the fluxes after the final, *N*th, iteration are given by F_k^N from (4.7), it can be shown from (2.9) that layers thinner than ε (which may be exceedingly small or even 0) will be precluded by the corrective fluxes given by the two vertical passes:

$$F_k^C = min\left[F_k^N, \Delta\rho_{k-1/2}max\left(\frac{h_{k-1,0}-\varepsilon}{\Delta t} + \frac{F_{k-1}^C}{\Delta\rho_{k-1/2}} + \frac{F_{k-1}^C - F_{k-2}^C}{\Delta\rho_{k-3/2}}, \quad and \right.\right.$$

$$\left.\left.\frac{h_{k-1,0}-\varepsilon}{2\Delta t} + \frac{F_{k-1}^C}{\Delta\rho_{k-1/2}}\right)\right] \tag{6.1}$$

$$F_k^{CC} = min\left[F_k^C, \Delta\rho_{k+1/2}\left(\frac{h_{k+1,0}-\varepsilon}{\Delta t} + \frac{F_{k+1}^C}{\Delta\rho_{k+1/2}} + \frac{F_{k+1}^C - F_{k+2}^C}{\Delta\rho_{k+3/2}}\right)\right], \tag{6.2}$$

with F_k^C in the uppermost layers and F_k^{CC} in the bottommost layers given by

$$F_1^C = F_1^I, F_2^C = F_2^I, F_{N-1}^{CC} = F_{N-1}^C, \text{and } F_N^{CC} = F_N^C. \tag{6.3}$$

The fluxes which are actually used are F_k^{CC}. These corrections will rarely be necessary, and even then the grace with which this scheme subsequently handles these vanishingly thin points is an indication of the robustness of this scheme.

The thickening bottom boundary layer in Fig. 6 is driven by interior shears due to bottom drag arresting the bottommost layer. In a three-dimensional flow, the bottom drag leads to a downslope Ekman transport that tends to thin the bottom boundary layer on the upslope side of a plume. In the real ocean much of the mixing within the bottom boundary layer is due to small scale turbulence, parameterizable with a friction velocity (Weatherly and Martin, 1978). This can be accommodated in isopycnal coordinate models quite easily by specifying the vertical profile of the diapycnal diffusivity. The potential energy increase due to diffusive entrainment by a layer is related to the diapycnal diffusivity of that layer by the simple expression
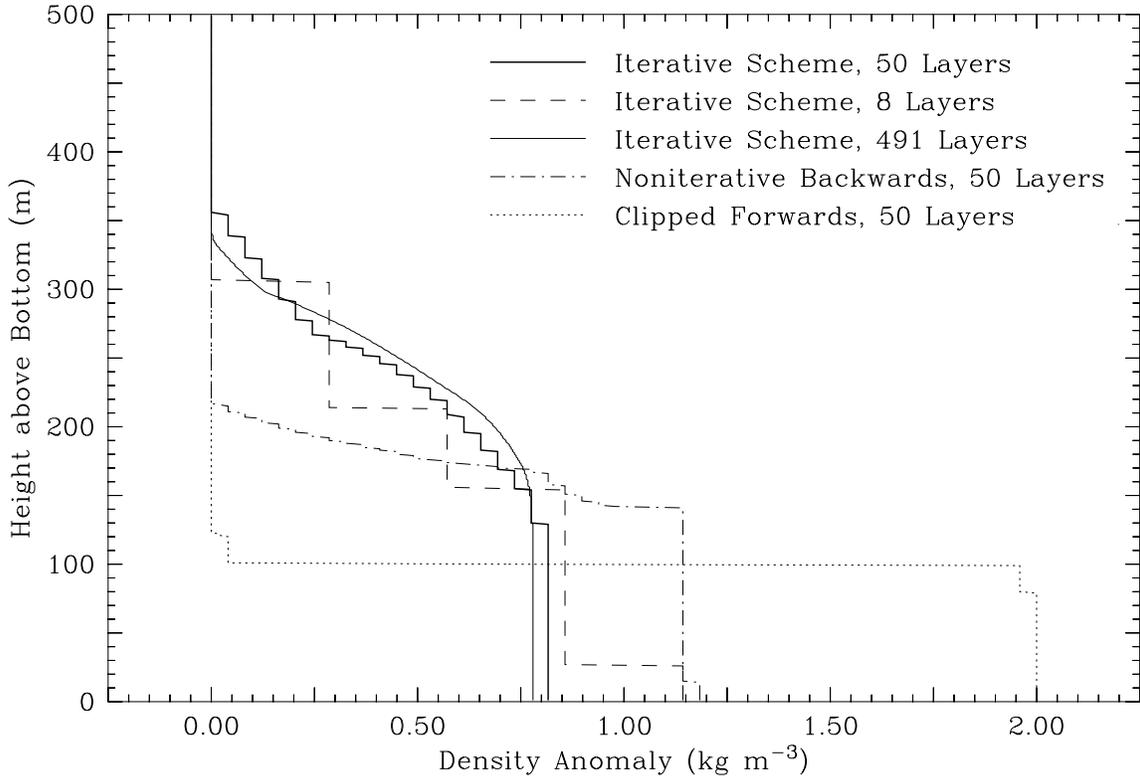
Figure 7. Density profiles after 3.5 days in the same simulation as depicted in Fig. 6 with several different time integration schemes and varying resolutions with the backwards vertically iterative scheme developed in this manuscript. The time step is 1 hour in each case except for the 491 layer iterative scheme simulation, where it is 2 minutes. The iterative scheme is described by (5.15), (5.16) and (4.7), while the noniterative backwards scheme is the same except for the vertical iteration described by (4.7), and the clipped forwards scheme is a simple forwards in time discretization subject to the constraint $F_k < \Delta\rho\sqrt{\kappa_{Background}/\Delta t}$. The 491 layer case uses 10 vertical iterations (more than enough to be fully converged at each time step), while the 50 and 8 layer iterative scheme cases use just a single vertical iteration.

$$\frac{\partial}{\partial t}(PE_k) = \kappa_k g \Delta\rho_k, \tag{6.4}$$

which is independent of the layer thickness, neighboring layer entrainment rates or any other property of the flow. So if a turbulent kinetic energy source at the bottom is specified, the corresponding diffusivity (perhaps accounting for the decay of turbulence away from the bottom boundary) can be applied to each layer, starting from the bottom, until enough layers are found to accommodate that energy source while still obeying the constraint to impose the boundary conditions, (4.3).

This technique for depicting the effect of the bottom source of turbulent kinetic energy will work well when the vertical resolution is sufficiently fine and the stratification is sufficiently high that the two bottommost layers are largely contained within the region of enhanced near-bottom turbulence. With less stratification or resolution, it is not possible to depict strongly bottom trapped

mixing (mixing within a density layer is by definition unrepresentable in an isopycnal layer model), and an appropriate bulk bottom boundary layer may prove beneficial. Still, microstructure observations by Polzen et al. (1997) indicate that the enhanced turbulent kinetic energy conversion to potential energy extends thousands of meters above the rough bathymetry on the flanks of the Mid-Atlantic Ridge in the deep Brazil Basin. If these observations are characteristic of the entire abyssal ocean, it is likely that a turbulent kinetic energy based parameterization of diapycnal diffusion will work well in an isopycnal coordinate model with adequate and judiciously chosen vertical resolution, and it may not prove necessary to have a separate bulk bottom mixed layer for many large-scale simulations.

The density profiles after 3 days show that the vertically iterative time integration scheme developed here is much more accurate than other alternatives, as seen in Fig. 7. One case with absurdly high resolution in density and time (491 layers and a 2 minute time step) using 10 vertical iterations is essentially converged. With the vertical iteration scheme (even with just 1 iteration) both the case with 50 layers and the case with 8 layers agree with the converged case. Another calculation (not shown) using the vertical iteration scheme with 50 layers and a 6 hour time step is virtually indistinguishable from the case with 50 layers and a 1 hour time step. A simple forward Euler time integration with the most generous flux limit that guarantees positive definite layer thickness entrains at a negligibly slow rate; the density at the bottom has not changed at all after 3 days, while in the true solution it is 60% of the way to the interior density. The backwards scheme without the vertical iteration also substantially underpredicts the amount of entrainment at this point, but at least it qualitatively resembles the converged solution, and that semblance improves with shorter time steps or fewer layers.

The utility of the diffusion scheme with the Richardson number dependent mixing can also be demonstrated with simulations from a fully three dimensional primitive equation isopycnal-coordinate ocean model. Water is initially all in the lightest layer, except in a bay at the top of a Gaussian slope in a reentrant channel. Within the bay, a sponge strongly restores the density towards a step-profile with the bottommost 150 m of water 2 kg m-3 denser than the remaining 350 m of water. 19 layers (20 interfaces), each differing in density from its neighbors by 0.1 kg m^{-3}, separate the lightest and densest layers. The dense water flows out of the bay at a rotating hydraulics controlled rate of about $(g20\Delta\rho/\rho)(150m)^2/f \approx 3.4\times10^6 m^3 s^{-1}$ and flows both down and along the slope. The horizontal resolution, 22 km, is not excessively high, but does permit adequate resolution of the slope and of the internal deformation radius of order 50 km. The 1 hour time step is appropriate for this horizontal resolution. The maximum slope is 1%. While these parameters are not intended to exactly reproduce any particular overflow, they are of a magnitude to be qualitatively illustrative of several important overflows.

The two simulations are identical except for the parameterization of diapycnal mixing. The one depicted in Fig. 8a uses a background diapycnal diffusivity of 1 cm^2 s^{-1}. The other simulation,
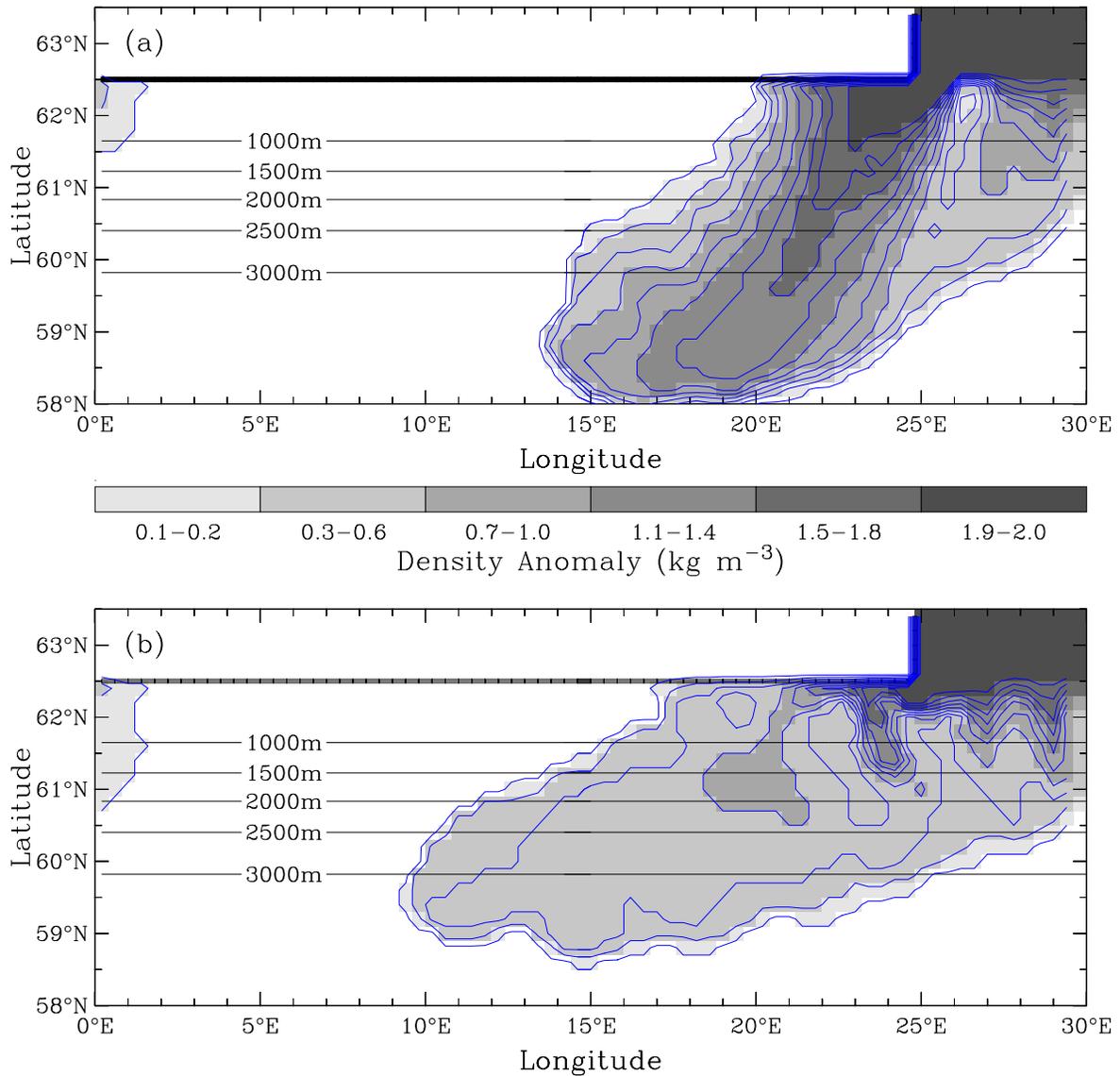
Figure 8. Density anomaly of the water 10 m above the bottom after 50 days in an entraining gravity current. In (a) a constant diapycnal diffusivity of 10^{-4} m^2 s^{-1} is used. In (b) the Richardson number dependent entrainment described in section 5 is used as well. The thin horizontal lines mark the isobaths of the Gaussian slope, the thick line marks the coast. The uncolored areas are at the initial, uniformly light density. Dense water is formed by a sponge in the bay in the northeast. The channel is reentrant, and the slightly dense fluid in the northwest corners of the basin is flowing eastward from the bay.

shown in Fig. 8b, also includes the Richardson number dependent mixing. Both use a single iteration of the vertically iterative time stepping scheme advocated in this manuscript, with a backwards Euler estimate of the diffusive entrainment by a single layer.

Without the Richardson number dependent mixing, a plume of nearly undiluted overflow water rapidly descends to the bottom of the slope. This is essentially the same behavior as was found with MICOM in the representation of the flow over the Denmark Strait in DYNAMO

(DYNAMO Group, 1997). The mixing that does take place is due to the explicit mixing parameterization and the spreading and thinning of the dense layer due to the divergent Ekman transport. This simulation, while not reproducing the ocean's behavior, does demonstrate the utility of the proposed time stepping scheme with a constant diffusivity in a difficult situation (the behavior at $\kappa \Delta t / h^2 \approx 1$ is important in this simulation) in a full three-dimensional ocean GCM. Halving the timestep causes only very minor changes in the result. This simulation also illustrates one great virtue of isopycnal models relative to other types of models for simulating gravity currents: there is not excessive numerical entrainment - all entrainment must be parameterized explicitly.

With the Richardson number dependent mixing, the dense water plume rapidly entrains to about 4 times its initial volume. The volume of dense water flowing out of the bay is the same in both cases, due to the robustness of the rotating hydraulic control, but essentially no dense water reaches the foot of the slope. Instead there is a very thick plume of strongly diluted water extending along the slope with the Richardson number dependent mixing. The behavior in this case is qualitatively similar to that seen in the open ocean (Price and Baringer, 1995). This simulation demonstrates that this Richardson number dependent mixing scheme alleviates the pathology in the representation of dense water overflows found with the isopycnal coordinate ocean model in DYNAMO.

It is actually very important for the large scale ocean circulation that the entrainment occurs with a sufficiently short time scale. Entraining gravity currents drop through the thermocline with a timescale of a few days (Price and Baringer, 1994) - if the time integration scheme does not permit entrainment to occur within that time, it is no longer possible for the gravity current to entrain thermocline waters. With insufficiently rapid entrainment, the overflows that contribute to intermediate or deep waters in the real world could easily wind up at the bottom of the ocean. A numerical ocean model which fills the abyssal Atlantic Ocean with Mediterranean overflow waters and the abyssal Indian Ocean with Red Sea overflow water would have limited credibility!

7. Conclusions

An implicit, vertically iterative time integration scheme for the diapycnal diffusion equations for an isopycnal coordinate ocean model has been proposed here. This scheme is stable with an arbitrarily large time step, accurate for well-resolved layers ($\kappa \Delta t / h^2 \ll 1$), and well behaved for thinner layers. This scheme is potentially much more efficient than the proposed scheme of Hu (1996a) because it can be implemented in two vertical passes through a column, and it does not impose a potentially unphysical limit on the intensity of mixing. This scheme is also more accurate than the entrainment scheme of Oberhuber (1993) for long time steps relative to the layer thickness divided by the entrainment rate because it permits interactions between many layers within a single time step. (Without any interactions between layers, the backwards scheme is equivalent to Ober-

huber's scheme.) The McDougall and Dewar (1998) treatment of separate temperatures and salinities and nonlinearities of the equation of state in isopycnal coordinate ocean models is entirely compatible with this technique. Repeated iteration in the vertical can improve the accuracy of the results, but even a single vertical iteration gives qualitatively reasonable results that are extremely accurate when $\kappa \Delta t / h^2 \ll 1$. The technique described here is qualitatively accurate in all situations that have been examined and is sufficiently efficient to be generally useful in isopycnal coordinate ocean models.

It should be reiterated that diapycnal mixing in an isopycnal coordinate model is only complex when stratification is large and mixing is intense. In the vast majority of the ocean's volume, the intrinsic timescales of diapycnal mixing are extremely long, and even the simplest time stepping scheme for diapycnal mixing works well. The approach suggested here is quite accurate in this limit, but it is substantially more costly than the simplest scheme.

The new implicit and vertically iterative time integration scheme works well with an appropriate Richardson number dependent entrainment parameterization, while non-implicit, noniterative time integration schemes are useless for accurate portrayal of entraining gravity currents with reasonable length time steps and modest to good density resolution. The important entrainment in gravity currents occurs with a timescale of only a few days (Price and Baringer, 1994), and any time integration scheme which does not permit the entrainment to occur within that time will lead to qualitatively inaccurate watermass properties throughout the deep ocean. While it has not been demonstrated here, the same Richardson number dependent entrainment should also be qualitatively reasonable in other regions of strong mixing driven by the resolvable scale shears, such as in the Equatorial Undercurrents.

The DYNAMO Group (1997) finds that their isopycnal coordinate ocean model lacks diapycnal mixing in the water just downstream of dense water overflows and concludes that "an improved representation of the bottom boundary layer in this regime should be of highest priority in the future development of all models". The Richardson number entrainment scheme described here is just such an improvement.

Bottom boundary layers are important for the larger scale ocean circulation primarily as sinks of momentum (and energy and potential vorticity and other related quantities) and for mixing that determines the watermass properties that fill the abyssal interior. Unlike the surface boundary layer, the exact temperature and salinity of a well homogenized bottom boundary layer is not important for most questions of climatic interest. It is entirely possible that an ocean model would have a satisfactory depiction of bottom boundary layer processes without attaching a separate bottom boundary layer model, provided that an appropriate level of mixing and an appropriate momentum sink are specified.

An appropriate level of near-bottom mixing cannot be specified in geopotential coordinate models without some sort of explicit bottom boundary layer model. Winton et al. (1998) have

shown that unless the *horizontal* resolution of a geopotential coordinate ocean model is finer than the bottom boundary layer thickness divided by the bottom slope, vastly excessive convective bottom mixing occurs in a dense downslope flow without an explicitly parameterized bottom boundary layer. Beckmann and Döscher (1997), Killworth and Edwards (manuscript submitted to *J. Phys. Oceanogr.*), and Gnanadesikan, Pacanowski, and Winton (manuscript in preparation) have all developed explicit bottom boundary layer parameterizations of varying complexity to be appended to geopotential coordinate ocean models, with a principle goal of controlling nonphysical diapycnal mixing. The fact that, in contrast, an isopycnal coordinate ocean model inherently has too little mixing means that it is possible to achieve an equally satisfactory result by adding diapycnal mixing in appropriate situations, but without all of the complications (such as having to unmix detrained fluid, thereby violating the second law of thermodynamics [Bleck et al., 1992]) of adding an explicit, variable density boundary layer model to the bottom of an isopycnal coordinate ocean model.

Isopycnal coordinate ocean models will never be as accurate as sigma coordinate models for simulating the structure of the bottom boundary layer. While a sigma coordinate model can enforce very high resolution near the bottom and incorporate high order turbulence closure schemes (Blumberg and Mellor, 1987), the resolution in isopycnal coordinates is automatically expelled from unstratified fluid. But isopycnal coordinates are in some ways well suited for describing the watermass modifications that are important for the large scale ocean density structure. The important dense overflows are typically much denser than the open ocean waters at the sill depth. If there is no resolution in density between the water flowing over a sill and the ambient interior water, this is only due to the *a priori* assertion in setting up the simulation that the distinction between these watermasses is not significant. In some ways an isopycnal coordinate model with Richardson number dependent mixing and a specified bottom turbulent kinetic energy source is ideal for depiction of the effect of the bottom boundary layer on the large scale ocean circulation; mixing in the absence of stratification is relatively unimportant, while stratified regions are automatically well resolved by the migrating isopycnal layers.

Acknowledgments

References

Beckmann, A., and R. Döscher, 1997: A method for improved representation of dense water spreading over topography in geopotential-coordinate models. *J. Phys. Oceanogr.*, **27**, 581-591.

Bleck, R. and L. T. Smith, 1990: A wind-driven isopycnic coordinate model of the North and Equatorial Atlantic Ocean. 1. Model development and supporting experiments. *J. Geophys. Res.* C, **95**, 3273-3285.

Bleck, R., C. Rooth, D. Hu, and L. T. Smith, 1992: Salinity-driven thermocline transients in a wind- and thermohaline-forced isopycnic coordinate model of the North Atlantic. *J. Phys. Oceanogr.*, **22**, 1486-1505.

Blumberg, A. F., and G. L. Mellor, 1987: A description of a three-dimensional coastal ocean circulation model. *Three-Dimensional Coastal Ocean Models*, N. Heaps, ed., **4**, Am. Geophys. Union, Washington DC, 1-16.

DYNAMO Group (S. Barnard, B. Barnier, A. Beckmann, C. W. Böning, M. Coulibaly, D. DeCuevas, J. Dengg, C. Dieterich, U. Ernst, P. Herrmann, Y. Jia, P. D. Killworth, J. Kröger, M.-M. Lee, C. LeProvost, J.-M. Molines, A. L. New, A. Oschlies, T. Reynaud, L. J. West, J. Willebrand), 1997: DYNAMO: Dynamics of North Atlantic models: Simulation and assimilation with high resolution models. Tech. Rep. Nr. 294, Institut Für Meereskunde an der Universität Kiel, Kiel, 334 pp.

Hallberg, R., and P. Rhines, 1996: Buoyancy-driven circulation in an ocean basin with isopycnals intersecting the sloping boundary. *J. Phys. Oceanogr.*, **26**, 913-940.

Hu, D., 1996a: The computation of diapycnal diffusive and advective scalar fluxes in multilayer isopycnic-coordinate ocean models. *Mon. Wea. Rev.*, **124**, 1834-1851.

Hu, D., 1996b: On the sensitivity of thermocline depth and meridional heat transport to vertical diffusivity in OGCMs. *J. Phys. Oceanogr.*, **26**, 1480-1494.

Jones, J. H., 1973: Vertical mixing in the equatorial undercurrent. *J. Phys. Oceanogr.*, **3**, 286-296.

McDougall, T. J., and W. K. Dewar, 1998: Vertical mixing, cabbeling and thermobaricity in layered models. *J. Phys. Oceanogr.*, **28**, 1458-1480.

Oberhuber, J. M., 1993: Simulation of the Atlantic circulation with a coupled sea ice-mixed layer-isopycnal general circulation model. Part I: Model description. *J. Phys. Oceanogr.*, **23**, 808-829.

Pacanowski, R., and S. G. H. Philander, 1981: Parameterization of vertical mixing in numerical models of tropical oceans. *J. Phys. Oceanogr.*, **11**, 1443-1451.

Pedlosky, J., 1996: Ocean Circulation Theory. Springer, New York, 453 pp.

Peters, H., M. C. Gregg, and T. B. Sanford, 1995: On the parameterization of equatorial turbulence: Effect of fine-scale variations below the range of the diurnal cycle. *J. Geophys. Res.* C, **100**, 18333-18348.

Polzen, K. L., J. M. Toole, J. R. Ledwell, and R. W. Schmitt, 1997: Spatial variability of turbulent mixing in the abyssal ocean, *Science*, **276**, 93-96.

Price, J. M., and M. O. Baringer, 1994: Outflows and deep water production by marginal seas. *Prog. Oceanogr.*, **33**,161-200.

Turner, J. S. 1996: Turbulent entrainment: the development of the entrainment assumption and its application to geophysical flows. *J. Fluid Mech.*, **173**, 431-471.

Wacongne, S., 1989: Dynamical regimes of a fully nonlinear stratified model of the Atlantic equatorial undercurrent. *J. Geophys. Res.* C, **94**, 4801-4815.

Weatherly, G. L., and P. J. Martin, 1978: On the structure and dynamics of the oceanic bottom boundary layer. *J. Phys. Oceanogr.*, **8**, 557-570.

Winton, M., R. Hallberg, and A. Gnanadesikan, 1998: Simulation of density-driven frictional downslope flow in Z-coordinate ocean models. *J. Phys. Oceanogr.* **28**, 2163-2174.

Yu, Z., and P. S. Schopf, 1997: Vertical eddy mixing in the tropical upper ocean: its influence on zonal currents. *J. Phys. Oceanogr.*, **27**, 1447-1458.